Submarine earthquake history of the Çınarcık Segment of the North Anatolian Fault in the Marmara Sea, Turkey

Authors

Laureen Drab,

Aurélia Hubert-Ferrari,

Sabine Schmidt,

Philippe Martinez,

Julie Carlut,

Meriam El Ouahabi

Address of corresponding author: Laureen Drab - ENS-laboratoire de Géologie- 24, rue Lhomond- 75234 Paris Cedex 05- France

Mail: drab@geologie.ens.fr

Abstract

The submarine part of the North Anatolian Fault (NAF) in the Marmara Sea is a significant hazard for the city of Istanbul (Turkey). The use of paleoseismological data to provide an accurate seismic risk assessment for the area is constrained by the fact that the NAF system is submarine near Istanbul; thus a history of paleoearthquakes can be inferred only by using sediment cores. Here a record of turbidites was obtained in two cores and used to reconstruct the earthquake history along a main branch of the NAF, the Çınarcık Segment. Core Klg04 (4 m long) was collected from a berm north of the fault and a second core (Klg03, 3.5 m long) was positioned in the Çınarcık Basin, 3 km south of the fault. Sedimentary sequences in the two cores were correlated using variations in Ca/Ti ratio, which reflect the local aquatic productivity compared with more terrigenous input. The turbidites between the two cores were then classified to distinguish the synchronous ones from the other ones. Radionuclide measurements suggest that the most recent turbidite recorded in both cores was triggered by the M=7.3 1894 earthquake. We conclude that the turbidites are earthquake-generated, based on: 1) their distinctive sedimentological and geochemical signatures, previously described and applied in the Marmara Sea; 2) on the correlation of turbidites between cores at berm and basin sites; 3) the match of the most recent turbidites with a 19^{th} century historical earthquake; and 4) the elimination of others processes. Because of its specific geomorphological location, Klg04 core likely records only mass wasting events related to the rupture on the Çınarcık Segment. To date older turbidites, we used ^{14}C and paleomagnetic data to build an OxCal age model with a local reservoir correction (ΔR) of 400±50 yr. The Çınarcık Segment is found to have ruptured in AD1894, AD1509, sometime in the 14^{th} century, AD989, AD740 and in the 5^{th} century and have a mean recurrence interval of rupture between 243 and 396 years. Following the age model obtained we finally used the earthquake record history of the Çınarcık Segment to infer the rupture history of adjacent segments of the North Anatolian Fault during six earthquake cycles over

the past 1500 years.

Introduction

Constraining the recurrence rate of M>7 earthquakes that threaten the megacity of Istanbul is problematic because the late Holocene faults are submarine. Istanbul, with 12 million inhabitants, borders the Marmara Sea (Fig. 1-a), a submarine pull-apart basin related to the North Anatolian Fault (NAF), a major strike slip fault that ruptures in large magnitude earthquakes. Since the M=7.4 1999 Izmit earthquake, stresses have further increased in the eastern part of the Marmara Sea (Hubert-Ferrari et al., 2000; Parsons et al., 2000; Pondard et al., 2007). Understanding past ruptures of the NAF in the Marmara Sea is thus a key issue in assessing seismic hazards for this area.

Sub-aqueous paleoseismology can reconstruct the history of large earthquakes on submarine faults (Goldfinger, 2011), as shaking associated with large offshore earthquakes triggers submarine landslides and turbidity currents. The resulting deposits can be sampled by sediment coring, characterized and dated. Earthquake-generated turbidites have generally been identified based on their synchronicity at different sites and their distinctive sedimentological or geochemical signatures (Gorsline et al., 2000; Shiki et al., 2000; Nakajima and Kanai, 2000; Beck et al., 2007; Masson et al., 2011; Drab et al., 2012). In the case of the Marmara Sea, several studies (McHugh et al., 2006; Sarı and Çağatay, 2006; Beck et al., 2007; Drab et al., 2012) have revealed that its sediments contain a record of turbidites triggered by large earthquakes. These turbidites have been used to constrain the history of earthquakes rupturing across a given depocenter (McHugh et al., 2006; Drab et al., 2012). The present study shows that sediment cores can be used to constrain paleo-ruptures of the fault segment located just south of Istanbul and to evaluate the recurrence rate of large magnitude earthquakes in this area.

Here, we apply sub-aqueous paleoseismology to two gravity cores located in the Çınarcık Basin of the Marmara Sea (Fig. 1). The Çınarcık Basin is located ∼20 kilometers to the south of Istanbul and is north-bounded by the Çınarcık Fault, the main segment of the NAF. In the two cores, we have identified and characterized different turbidite deposits. We also used global changes in sediment pattern to correlate the two records to a reference core located in a non-turbidite depositional environment. Finally, we investigated the origin of their specificity, the specific core location and their granulometric and geochemical characteristics. Radiogenic lead and cesium data allowed us to match the turbidites at the top of the sediment columns with recent historical earthquakes. Radiocarbon dating combined with paleomagnetic data enabled us to construct an age model for the Klg04 sediment core located in a berm in the Çınarcık Fault scarp (Fig. 1-c) and to date turbidites over the last 1500 years. The obtained chronology could then be used to examine the changes in sedimentation rate in the Çınarcık Basin. Finally, the NAF rupture behavior in the Marmara Sea is discussed.

Setting

Tectonic and paleoseismological background

The North Anatolian Fault is a major dextral strike slip fault extending over 1200 km in northern Turkey and in the Aegean Sea (Barka and Kadinsky-Cade, 1988; Sengör et al., 2005) (Fig. 1-a). In the Marmara Sea, the NAF accommodates a horizontal motion of 25 mm/yr (Reilinger et al., 2006) spread over a width of 130 km (Barka and Kadinsky-Cade, 1988). Most of the deformation is localized on the northern branch of the NAF (McClusky et al., 2003), which crosses the Marmara Sea. The Marmara Sea is 170 km long, has a maximum water depth of 1250 m and is composed of three aligned pull-apart basins separated by two topographic ridges (Le Pichon et al. (2001); Armijo et al. (2002); Sarı and

Çağatay (2006); Fig. 1-b).

The study focuses on the Çınarcık Basin, the easternmost transform basin of the Marmara Sea (Fig. 1-c). The 50 km long x 18 km wide basin is bounded to the North by the main segment of the NAF and to the South by a secondary normal fault system (Le Pichon et al., 2001; Smith et al., 1995; Armijo et al., 2002). The main northern segment, here called the Çınarcık Segment, runs at the base of a steep escarpment, 1000 m high (from 200 mbsl to 1200 mbsl) and 40 km long. The fault is characterized by composite strike slip and normal motions (Armijo et al., 2002).

In the last 300 years, the Çınarcık Basin has experienced several M>6 earthquakes (Ambraseys (2002); Fig. 1-a). The most recent Mw=6.3 1963 earthquake occurred on the southern fault bordering the Çınarcık Basin (Bulut and Aktar (2007), Fig. 1-a). Presently, this is the only earthquake unambiguously attributed to a fault in the Çınarcık Basin. The M=7.3 1894 earthquake has been located in the Çınarcık Basin (Parsons, 2004; Hebert et al., 2005; Pondard et al., 2007) or in the Izmit Bay (Hubert-Ferrari et al., 2000; Ambraseys, 2002; McHugh et al., 2006). The associated tsunami strongly affected the Prince Islands, south of Istanbul (Ambraseys, 2002; Altınok et al., 2011). During the 18th century there was a westward propagating sequence of earthquakes in the Marmara Sea (AD1719, AD1754, May and August AD1766), but the corresponding fault ruptures are poorly constrained. In AD1509, a large earthquake destroyed Istanbul; its epicenter has been located near the city (Ambraseys, 2001, 2009) but it may have ruptured either the Çınarcık or the Central Faults (Guidoboni et al., 1994). Destruction associated with the AD1343 earthquake was mostly on the western part of the Marmara Sea, but this earthquake was associated with a large burst of seismicity during the end of the 13th and 14th centuries in the Marmara Area (Ambraseys and Finkel, 1991). The AD989 earthquake principally affected the Istanbul Region with a tsunami reaching the city (Ambraseys and Finkel, 1991; Altınok et al., 2011). Historical data predominantly locate the event in the Çınarcık Basin

(Ambraseys, 2002; Guidoboni et al., 1994). Finally, the M= 7.1 740 earthquake was associated with a large tsunami (Altınok et al., 2011). It was mainly located in the Çınarcık Basin (Ambraseys, 2002; Guidoboni et al., 1994) but some authors have suggested an epicenter location in the Izmit Bay or Central Basin (McHugh et al., 2006; Bertrand et al., 2011; Çağatay et al., 2012). Historical information is limited for older ages but Ambraseys (2002) located the 407 and 437 earthquakes in the Çınarcık Basin.

Based only on historical reports it is difficult to unambiguously associate an offshore earthquake with a given submarine fault (Table 1). Even studies combining historical data with attenuation laws models (Parsons, 2004) or distribution of slip deficit and coulomb stress interaction (Pondard et al., 2007) propose different rupture scenarios across the Marmara Sea. Sub-aqueous paleoseismology studies do provide additional constraints. Indeed, in the Marmara Sea, earthquake-triggered turbidites have been documented by McHugh et al. (2006), Sarı and Çağatay (2006), Beck et al. (2007) and Drab et al. (2012). In addition McHugh et al. (2006) and Drab et al. (2012) found that large earthquakes rupturing the bounding or crossing fault of a given basin strongly affect its sedimentation, but have minor or no effects on the nearby sedimentary basins. Thus, a series of individual seismoturbidites can be linked to a specific earthquake rupture associated with large historical earthquakes.

Seismo-turbidite characteristics

In general, turbidites are assumed to have a seismic trigger because of their broad contemporaneous occurrence in a given setting (Goldfinger, 2011) and of their particular sedimentological imprint. In the Marmara Sea, the geographical extent of turbidite deposits have been deduced by correlating different sediment cores or by using very high-resolution seismic sub-bottom profiles for imaging the thickest mass-wasting deposits (McHugh et al., 2006; Beck et al., 2007).

The simultaneity of turbidite deposition in cores can be readily inferred in the Marmara

Sea because Holocene sedimentation displays simultaneous changes. Most of these changes are related to anthropogenic disturbances (Drab et al., 2012). Deforestation, which began 4 kyr ago (Mudie et al., 2007), triggered an increase in sedimentary flux to the Marmara Sea (Walling, 2006). Later changes in vegetation and land use strongly affected Marmara Sea catchments and southern shelf (Kazanci et al., 2004; Mudie et al., 2002), and very likely also affected the sedimentation in the deep basins (Mudie et al., 2007). Drab et al. (2012) have shown that global sedimentological changes in the Marmara Sea can be tracked through X-Ray Fluorescence (XRF) measurements. In particular, the Ca/Ti ratio, representing the local production (Ca) with respect to the allochthonous input (Ti), shows similar variations in basins and highs. For example, the ratio shows identical fluctuations in the Western High and in the Çınarcık Basin despite the different structural settings and the occurrence of distinctive small turbidites in the Çınarcık Basin (Drab et al., 2012). As a consequence, common time horizons between the different sediment cores can be linked to correlate turbidites in a given depocenter.

Seismoturbidites are also generally distinctive from non earthquake-triggered slope failure turbidites because of their specific sedimentological and mineralogical imprints. They are characterized primarily by complex laminae (Shiki et al., 2000; McHugh et al., 2011), sharp basal layers (Shiki et al., 2000), multiple coarse bases enriched with shells and detrital material indicating multiple sources (Nakajima and Kanai, 2000; Bertrand et al., 2008; Goldfinger et al., 2008), variation in the composition of detrital material between each event (Nakajima and Kanai, 2000) and abrupt changes in sedimentary structures (Nakajima and Kanai, 2000; Shiki et al., 2000).

Seismoturbidites in the Marmara Sea have been distinguished from other turbidites based on their particular grain size and geochemical characteristics (Sarı and Çağatay, 2006; Beck et al., 2007; Çağatay et al., 2012). The seismoturbidites deposited in the Central and Tekirdağ Basins have the following specific characteristics (Drab et al., 2012): 1) They display non-gradational changes in particles size and coarse basal pulse; 2) intermediate silt-rich layers show numerous thin parallel laminae linked to oscillating currents (Beck et al., 2007; Campos et al., 2013); 3) sharp basal sand layers are characterized by a decrease in bromine (Br) content, a relative increase in titanium (Ti), a peak in zirconium (Zr) and magnetic susceptibility (Çağatay et al., 2012; Campos et al., 2013); and 4) the turbidite is capped by a clayey silt layer. Turbidites induced by earthquakes in the Izmit Gulf have the same characteristics and show a large peak in manganese below the base of the turbidite related to a transient reduction front following the turbidite deposit (Çağatay et al., 2012). Finally, these seismoturbidites are synchronous with distal fine-grained deposits in the adjacent Western High that are related to a thick suspension cloud above the turbidite flow (McHugh et al., 2011; Drab et al., 2012).

In the Çınarcık Basin, the record of turbidites has not been studied in detail yet, but Sarı and Çağatay (2006) have identified reworked deposits in sediment cores and have inferred a seismic trigger due to: 1) the increase in different detrital material at the base of their events; 2) the occurrence of shallow benthic foraminifers; and 3) the exclusion of any other possible triggering mechanism.

Coring Site and Methods

Two Kullenberg sediment piston cores, Klg03 and Klg04, were collected in the Çınarcık Basin during the Marmarascarps cruise in 2002 (Armijo et al., 2005) shortly after the M=7.4 1999 Izmit earthquake (Fig. 1-a). They are 3 km apart and lie along the Çınarcık Fault Segment bordering the northern edge of the basin. Core Klg03 is located in the deepest part of the main Holocene depocenter (1240 mbsl)(Carton et al., 2007), 1.6 km south to the main fault strand. The site is on the main path of turbidites coming from the northern shelf, but it can also be reached by turbidites generated on the Central High or on the southern slope (Fig. 1-c). Core Klg04 is located in a topographic berm between two splays of the Çınarcık Segment near the base of the 1000 m high northern slope in front of the Prince Islands (Fig. 1-c). It lies 300 m north of the main fault segment and is 35 m higher than the Klg03 site (Fig. 1-d). Because the Klg04 site is placed significantly above the basin floor, it can be reached only by turbidites originating from the northern shelf.

A number of sedimentological investigations were performed to describe and characterize turbidites in the cores. X-ray radiographs obtained on the scopix system at Environnements et Paloenvironnements Ocaniques et Continentaux (EPOC) research group in University of Bordeaux were used to identify turbidites, similar to Beck et al. (2007) and Drab et al. (2012). Grain size measurements were performed on bulk sediment every centimeter on a Malvern Mastersizer 2000 to support the identification of turbidites (Folk, 1968; Sperazza et al., 2004; Bertrand et al., 2008). Magnetic susceptibility measurements were obtained on split cores using a Bartington MS2E every 5 mm at room temperature and highlight beds enriched in coarse detrital material (Fe, Mg, Ti), which can characterize the base of turbidites (Butler, 1992; Tauxe, 2010). XRF data were acquired using X-ray fluorescence on an Avaatech XRF core scanner and were used to describe geochemical and sedimentological processes associated with earthquake-related deposits by comparing elements considered as detrital with more local ones, like calcium. Measurements were taken every 5 mm with radiation energies of 10 keV and 30 keV to reach a large spectrum of elements comprising Ca, Ti, Mn and Zr. The elemental distributions were standardized to have a zero mean and unit variance to compare the variation of intensity through the sediment cores. We also used ratios of elements that provide the most easily interpretable signal of relative changes in chemical composition, and minimize the risk of drawing erroneous conclusions by enhancing the signal-to-noise ratio (Palike et al., 2001; Vlag et al., 2004; Bahr et al., 2005).

The chronology of the sediment cores is based on ^{210}Pb, ^{137}Cs and ^{14}C analyses and paleomagnetic measurements. The ^{210}Pb and ^{137}Cs radionuclides were measured using a semi-planar γ detector at EPOC, University of Bordeaux 1 (Schmidt et al., 2009). Paleomagnetic measurements (secular variation of the inclination and declination) provided independent time constraints. The Natural Remanent Magnetization (NRM) was measured on 1.5 m-long U-Channel samples cut from cores using a horizontal cryogenic magnetometer 2G-enterprise at the paleomagnetic laboratory of the Institut de Physique du globe de Paris (IPGP). Measurements were performed every 2 cm. The NRM was progressively demagnetized using an alternating field in 11 steps up to a maximum field peak of 90 mT on Klg04. The characteristic remanent magnetization (ChRM) was then isolated using Zijderveld diagrams and least square principal component (Kirschvink, 1980; Cogné, 2003). Zijderveld diagram will be presented in the Appendices. Core Klg03 was also analyzed, but only two demagnetization steps were applied because of technical issues.

AMS radiocarbon dating on 24 samples (benthic foraminifers, planktonic foraminifers and mollusk shells) was carried out at Artemis LMC14 laboratory in LSCE, Orsay and at the Aeon laboratory (Table 2). Both planktonic and benthic foraminifers were collected when possible in hemipelagic sediments just above the turbidites. Mollusk shells were mostly extracted at the base of turbidites. Samples were selected in the first 150 cm of the two sediment cores in order to be able to relate recorded turbidites with historical earthquakes whose segment ruptures may not be well constrained. Ages were calibrated using OxCal calibration software with the Marine13 calibration curve (Reimer et al., 2013). Because two different samples types (mollusk shells and *G. Bulloides* planktonic foraminifers) collected at the same depths (160 cm and 350 cm) gave the same ^{14}C age (Table 2), we assumed that the reservoir effect is the same for shells, planktonic and benthic foraminifers over 2000 years BP.

Results

Sedimentology, physical and chemical properties of turbidites

Visual inspection shows that all sediment cores have a very uniform silty-clay lithology with few sandy laminae containing shells fragments (indicated by a rectangle on the left side of the log in Figures 2 and 3). However, X-ray imagery combined with grain size measurements indicate that sediments are composed of a succession of rapidly deposited layers, e.g. turbidites. The turbidite deposits are characterized by a basal dark gray sandy layer progressively grading to a grayer silt layer and in places to a light gray clayey layer. The sand layer displays collocated high magnetic susceptibility and zirconium values as well as a peak of manganese below the basal layer (Figs. 2, 3 and 4, Çağatay et al. (2012)). All of the sandy bases in Klg04, and 98% of those in Klg03, display a sharp lower boundary, some of which is irregular, indicating erosion associated with strong disturbances in the sediment structure (see cartography of X-ray on the right side of the log in Figures 2 and 3). This sandy base also appears in 50% of the turbidites in Klg04 and 30% in Klg03 multiple pulses (Figs. 2, 3 and 4-b). The overlying silt layer in Klg03 frequently shows numerous thin parallel laminae, greater in concentration near its base. Beck et al. (2007) have linked these laminae to the to-and-fro bottom displacement induced by oscillating earthquake-triggered currents. In Klg04, the overlying silt layer exhibits mostly turbulent deposition. In both cores, the intermediate silt layer reaches a maximum just above the basal layer and slowly decreases up to a minimum or stays nearly constant. The light-gray clayey layer, which caps some sequences shows possible traces of bioturbation but is not easily distinguishable from hemipelagic sediments.

In core Klg03, we also identify a few proportions of sandy layers that do not show an erosive base (named tA, tB, tC and tD in Figure 2); these turbidites only contain laminae that are 2 to 5 cm thick. In addition, very thin sand laminae (∼2 cm thick) that may correspond to minor turbidites are observed in the sediments. They typically have less than half of the thickness of the smallest major turbidite (∼5 cm) identified in the same core.

Turbidite deposits comprise about 50-60% of the sediment record of Klg03 and Klg04 cores. The 370 cm-long Klg03 core shows fourteen erosive base turbidites, with thicknesses ranging from 5 cm to 18 cm, and four non-erosive base turbidites (Fig. 2). Twenty-three turbidites are recorded in Klg04, with thicknesses ranging from 8 cm to 20 cm (Fig. 3).

Cores and turbidites correlation

The two cores were correlated based on the variation of Ca/Ti ratio (Bahr et al., 2005; Gracia et al., 2010). In the Marmara Sea, global variations in the Ca/Ti ratio are related to environmental changes - for example, variation in soil erosion due to land use and cover changes (Drab et al., 2012) and, in the Çınarcık Basin, are independent of turbidite deposits. Indeed, no short-term changes in Ca/Ti, reflecting variations in grain-size within the turbidites, are observed (Fig. 4); titanium is not enriched in either the sandy or the silt-size fraction of the turbidites, contrary to what is usually documented (e.g.,Cuven et al. (2010)). The Ca/Ti ratio is thus used here to define similar time horizons between the two cores with respect to a reference core, Klg06, located in the Western High, 100 km away of the Çınarcık Basin (Figs. 1 and 5). Because of its specific structural position, Klg06 does not contain a record of coarse-grained turbidites like the ones deposited in the three basins of the Marmara Sea (Drab et al., 2012). This time correlation allows for the comparison and correlation of turbidites recorded in Klg03 and Klg04 independently of the age model derived using radiocarbon data (Figs. 5 and 6).

Twelve tie points are defined between the Klg06 record and the Klg03-Klg04 cores (Fig. 5). The correlation highlights that: 1) Klg04 and Klg06 span a similar time frame (6.5 kyr according to radiocarbon data), while Klg03 records only the last 4 kyr; 2) a 25 cm-thick erosional event occurred at a depth of 80 cm in core Klg04; 3) all turbidites recorded in Klg04 extend to Klg03 and are recorded at Klg03 site; and 4) Klg03 displays more turbidites than Klg04 during the same time interval. The turbidites common to Klg04 and Klg03 are addressed as events marked with a capital E. The erosional event in Klg04 correlates with the turbidite t5 in Klg03. The event is considered synchronous between the two cores and is called E5. We thus defined eleven synchronous events (Fig. 6). Within core Klg03 we observed that the turbidites linked with turbidites in Klg04 always displayed sand visible to the naked eye (Fig. 6). This suggests that the synchronous turbidite deposits in Klg03 have a near-field origin while the others may have a far-field origin. The nearest slope-failure sources are the northern slope and the shelf of the Çınarcık Basin (Fig. 1-c). This reasoning further leads us to identify the source of the events deposited simultaneously at the Klg04 and Klg03 sites. The Klg04 sediment core (1206 mbsl) is located in a berm, 35 m higher than the Klg03 site (1241 mbsl), near the base of the 1000 m high northern slope (Fig. 1-d). Because of its particular geomorphologic location, only mass-wasting events coming from the north would be recorded at this site. On the contrary the Klg03 core is located on the basin bottom in the area where the sedimentary infill is the thickest (Carton et al., 2007). Mass-wasting events triggered by slope destabilizations from the different sides of the basin (see arrows showing mass-wasting paths in Figure 1-c, Altınok et al. (2011)) would reach the Klg03 site more easily. The non-sandy Klg03 turbidites disconnected from the Klg04 ones are, in the present context, interpreted to have a distal source located on a far-field slope of the Çınarcık Basin. Our study will thus focus mostly on the turbidites synchronous between Klg03 and Klg04.

Chronology

Chronology of recent events based on $^{210}Pb_{xs}$ and ^{137}Cs activities

The age of the turbidites in the upper 50 cm of Klg03 and 25 cm of Klg04 can be constrained using unsupported ^{210}Pb, the derived product of ^{222}Rn that diffuses as gas through the atmosphere, and ^{137}Cs data. In Klg04, the basal layer of turbidite t1 is identified at 12 cm (Fig. 7). The turbidite has an erosive base and shows a sharp and strong increase in grain size. In Klg03, a turbidite with an erosive base is identified at 45 cm (labeled t1 in Fig. 7). Turbidite tA shows strong laminae and no erosive base along with a minor broad rise in mean granulometry, a high magnetic susceptibility peak and an increase in zirconium content (Fig. 3). Turbidite t1 in Klg03 has similar characteristics to t1 in Klg04. A third minor disturbance, 8 cm thick, is also visible in the X-ray at 30 cm in Klg03 (Fig. 6). It is marked by sand and small Zr peaks and is mainly characterized by disturbed clayey-silt layer.

In Klg04, the ^{137}Cs chronology shows a first peak at 2 cm depth and a second at 8 cm. The first peak can be related to the 1986 Chernobyl event and the second to the 1963 peak in atmosphere nuclear testing (Lima et al., 2005; van Welden et al., 2008). Unsupported ^{210}Pb is consistent with the cesium trend and exhibits, in the first 10 cm, an exponential decay with increasing depth (black circles in Figure 7). Radionuclides activities are also consistent with those of the nearby ROV (Remote Operation Vehicle) short cores collected during the same cruise (Uçarkuş (2010); white circles in Figure 7). We calculated the background sedimentation rate using the Constant Flux - Constant Sedimentation model (Robbins, 1978). This model assumes that the excess ^{210}Pb in the atmosphere and in its sedimentation rate are constant through time. When these assumptions are satisfied, the ^{210}Pb varies exponentially with depth and a sedimentation rate can be calculated. For Klg04, the deduced background sedimentation rate is 0.12 cm/yr. By extrapolation, turbidite t1, 12.5 cm in depth, is inferred to have occurred between AD1876 and AD1894, as the top of the core corresponds to year of sampling, 2002.

In core Klg03, the ^{137}Cs profile shows a peak at 23 cm, possibly related to the 1963 peak in aerial nuclear testing (Fig. 7). The uppermost 25 cm also displays a constant and high ^{210}Pb activity in an inferred reworked layer. ^{137}Cs and ^{210}Pb data imply that turbidite tA occurred very recently and may be related to the 1999 Izmit earthquake. The small disturbance detected at 30 cm depth might have been triggered by the 1963 Çınarcık earthquake. Below 25 cm, ^{210}Pb activity displays a rapid exponential decay until 40 cm and we deduced a background sedimentation rate of 0.13 cm/yr using the Constant Flux Constant Sedimentation model. Low values in ^{137}Cs that would occur before aerial nuclear testing around 1954 are reached at 36 cm. The age of turbidite t1 (45 cm) was calculated using the mean sedimentation rate of 0.13 cm/yr obtained with ^{210}Pb from the depth of 36 cm, corresponding approximately to the year 1954. Turbidite t1 would have been deposited between AD1875 and AD1886.

Radionuclide data imply that turbidite t1, recorded at 12 cm depth in Klg04 and at 45 cm in Klg03, has an age of around AD1880-AD1890, and thus probably the same trigger (Event E1 in Figure 6). The M=7.3 1894 Prince Islands earthquake occurred at that time in the Çınarcık Basin. We thus infer that this large historical earthquake triggered the Event E1 in both cores.

Chronology based on Paleoinclination data

Paleoinclination and paleodeclination data were obtained on both cores to provide independent age constraints. Data were only analyzed when the NRM intensities presented values greater than 1.10^{-2} A/m, indicating a good preservation of the magnetic signal. This corresponded to the first 80 cm in Klg04 and to the interval 80 and 190 cm in Klg03 (Fig. 6). The presence of turbidites implies that our record is discontinuous and affects the magnetic signal. We thus removed data from all the sandy bases of the turbidites considered to be unreliable due to strong grain size variation. We then calculated a mean value for the silt and clay layers. These average values were interpreted to represent paleoinclination and paleodeclination at the time of, and just after, turbidite deposition, respectively. Finally, all of the data were kept for the hemipelagic sedimentation.

The paleoinclination and paleodeclination data were compared to the reference curve of secular variation in inclination and declination computed at the latitude of coring site for the last 2000 years (Korte and Constable, 2011) and with a local curve obtained in the Balkans (Tema and Kondopoulou, 2011) (Fig. 8). We focused mostly on core Klg04, which has a more robust data set than Klg03. The Klg03 record is also included as it shows a secular variation of geomagnetic field similar to Klg04 and because the dataset covers a longer time frame than Klg04. Therefore, it provides additional time constraints. The fact that the Klg04 record and the reference curves present exactly the same pattern in inclination and declination supports the reliability of the record.

Klg04 mean inclination is close to expected values (54°), and magnetic inclination minima and maxima can be identified. The Klg04 mean inclination presents similar variations to the reference models for the last 2000 years with corresponding periods of low and high inclination. A direct comparison of the relative ChRM inclination of core Klg04 and the computed inclination from the model allows for the determination of four common paleomagnetic inclination features (N0, N1, N2, N3 in Figure 8). Events E2 and E3 occurred during the low inclination period N2 and event E4 and the main erosional event, E5, occurred at the end of the high inclination values of the N3 period (about 500 cal years).

Declination in Klg04 exhibits the same trends as the reference curve and three periods with identical trends can be identified (D0, D1 and D2). Events E2 and E3 were deposited during the period D2, between 1500 and 1000 cal years, while event E4 occurred before the large decrease in declination around 800 cal years, suggesting that this turbidite may have been deposited between 1000 and 800 cal years. Four turbidites are thus recorded in about 1000 cal years. This result was used as a chronological marker to derive the reservoir age for the Çınarcık Basin.

The Klg03 and Klg04 records present a similar pattern in inclination and declination, even if the inclination in Klg03 is shallower, indicating a possible tectonic disturbance or a mechanism of inclination shallowing (Tauxe and Kent, 1984). The comparison with the reference models allows for the matching of paleomagnetic changes between core Klg03 and the reference curves, as we have done for Klg04 (e.g., inclination periods N2 and N3; declination period D2). Klg03 records the low inclination period N4, the high inclination period N5, as well as the low declination period D3 (Fig. 8). Event E5, like E4, occurred during the high inclination period N3; event E6 occurred at the beginning of the low declination period D3 and during the low inclination period N4. This suggests that E6 was deposited between AD400 and AD0.

Paleomagnetic measurements obtained on the Klg03 and Klg04 cores also display important variations in the magnetic properties. A drop of magnetization in the NRM data is observed at 250 cm in Klg03 and at 80 cm in Klg04 (Fig. 6) and corresponds to the dissolution of magnetite grains through the process of diagenesis in the sediment. The origin of the magnetic drop has been extensively studied by Drab (2012). The occurrence of the very low magnetization is linked to the deposition of organic-rich material forming a sapropelic layer (Cramp and O'Sullivan, 1999; Larrasoaña et al., 2003). These organic-rich layers are commonly found in the Mediterranean Area (Rohling and Hilgen, 1991; Cramp and O'Sullivan, 1999; Larrasoaña et al., 2003) and in the Marmara Sea (Çağatay et al., 2000; Tolun et al., 2002; Vidal et al., 2010). The last referenced sapropelic layer was identified by Çağatay et al. (2000) and occurred between 4.7 kyr and 3.2 kyr in the Marmara Sea. We identified in Klg03 and Klg04 this sapropelic layer by an increase in Total Organic Carbon content and by the sharp decrease in NRM intensity at 250 cm and 150 cm depth, respectively. The layer is mapped in Figure 6 and can also be used as an independent time constraint for the core chronology.

Chronology of seismoturbidites based on radiocarbon data

To determine the age of turbidite deposits, we used an OxCal model with unrounded ages (Reimer et al., 2013). The software derives modeled probability density functions (PDFs) of the samples and sedimentary events (Fig. 9). We used only stratigraphic ordering constraints and did not consider models with a continuous background sedimentation rate in between mass-wasting deposits because some erosion likely occurred at the base of turbidite flow. However, boundaries were applied as in Kagan et al. (2010) when a major change in sedimentation was suspected. The top boundary of the model is constrained by the age of the 1894 earthquake, which radionuclide measurements imply, corresponds to event E1. Time constraints were also applied using the top of the upper sapropelic layer and the secular variation of the magnetic field.

The ^{14}C-based age model was constructed with 24 samples and three paleomagnetic age constraints (sapropelic layer and three approximate calendar ages). All the ^{14}C data obtained from core Klg03 were applied to core Klg04 based on the detailed Ca/Ti correlation (Figs. 5 and 6). Seven samples (Klg04-91 cm, Klg04-162 cm, Klg04-184 cm, Klg04-197, Klg04-214 cm, Klg03-88 cm and Klg03-114-plc cm) largely overestimated the expected age of the host sediment. These samples were regarded as being reworked and were not used in the model (indicated in italic in Table 2). Samples extracted from the sandy base of the turbidites (Klg04-38cm, Klg04-45.5cm, Klg04-59cm, Klg03-98cm, Klg03-203.5cm and Klg03-245cm) were assumed to be reworked material incorporated into the mass-flow. They are considered to predate the turbidite deposit and were incorporated in a phase function as in Lienkaemper and Ramsey (2009). Finally, 17 radiocarbon samples were used to make an order-constrained Bayesian model using the OxCal software (Reimer et al., 2013).

Obtaining an age model is complicated in marine environments because of the presence of a radiocarbon-depleted signal within the oceans (Siani et al., 2001; Reimer and McCormac, 2002). Indeed, the ocean is a large carbon reservoir and has a longer residence time for ^{14}C than the atmosphere. Radiocarbon ages obtained from marine shells thus have an apparent age older than atmospheric samples. The marine reservoir age is defined as the difference between ^{14}C samples from marine and terrestrial material of the same age (Stuiver et al., 1986) and is composed of a global reservoir correction R (about 400 years) and a local deviation (ΔR) that can be as large as 1000 years (Stuiver et al., 1986). To obtain an accurate chronology in marine environment, the key issue is thus to assess the right reservoir age. The only data pertaining to the Marmara Sea were obtained by McHugh et al. (2006). The authors constrained the ^{14}C ages of modern pre-bomb marine mollusk shells of the Marmara Sea and calculated a total average age reservoir of 460±40 yr (ΔR 71) and 340±40 yr (ΔR 91), following Siani et al. (2000).

We combined radionuclide, radiocarbon and paleoinclination data at the top of Klg04 to calculate the most suitable marine reservoir correction (Fig. 9). Possible variations in reservoir age overtime were ignored because of lack of data to address this problem (Goldfinger et al., 2012). Radionuclide dating suggests that the turbidite E1 at 12 cm was deposited in the 1890's. The radiocarbon age of the foraminifera sample (1060±30 yr BP at 17 cm) just below event E1 implies a large reservoir age of about 900 years (Table 2). The direct comparison between the chronostratigraphic markers in declination, inclination and radiocarbon ages of Klg04 samples presented in Figure 6 confirms that a total reservoir correction between 800 to 900 years is needed. We therefore applied a local reservoir deviation (ΔR) of 40050 yr to the marine calibration curves in OxCal. The results are presented in Figure 9 with 95% age probability (2σ). Events E2, E3 and E4 have 2σ calendar age ranges of AD1288-1664, AD1178-1399 and AD710-1164, respectively. The OxCal model also constrains the age range of the four other events at AD399-867 (Erosion Event, E5), AD20-AD512 (E6), BC413-AD165 (E7) and BC1318-BC755 (E8). The order-constrained Bayesian model was also used to determine an average recurrence interval of 243 to 396 years for turbidites synchronous at both sites. This average recurrence interval is in good agreement with the recurrence interval that can be calculated from inclination data (250 years).

Discussion

Timing and causes of changes in sedimentation rates

Comparing sediment accumulation through time at the two sites provides some insights about major changes in sedimentation rates in the Çınarcık Basin over the last 4000 years. Despite the differences in the turbidite occurrences, the two cores have similar accumulation rate curves and show identical major changes in sedimentation pattern (Fig. 10). Five periods with different sedimentation rates are recorded. The chronology allows for the discussion on their origins.

A strong anomaly occurred in the 140-220 cm interval in Klg04, and below the depth of 250 cm in Klg03. During this period labeled P4, sedimentation rates are similar at the Klg03 and Klg04 sites, but exceptionally high (0.23 cm/yr in Klg04 and 0.4 cm/yr in Klg03). In the OxCal model, the P4 period occurred between BC1100 and BC1500 and is coincident with the occurrence of the upper sapropelic layer referenced between 4.75-3.2 kyr BP by Çağatay et al. (1999) in the Marmara Sea. Sapropelic layers are characterized by good preservation of the organic material in a reductive environment (Cramp and O'Sullivan, 1999). One way that sapropels are formed involves the slowing down of oxygen flux in the sediment and the most effective process to reduce bottom water ventilation is to have a high sediment influx (Calvert, 1990; Çağatay et al., 2004). The high sedimentation rate during this period could also be related to the beginning of forest clearance and crop agriculture in the Marmara watersheds, starting at BC1450 cal years (Eastwood et al., 1998; Leroy et al., 2002); indeed a peak in sedimentation rate is documented in lakes and along the southern shelf of the Marmara Sea at that time (Kazanci et al., 2004).

However, during the P4 period, about five turbidites are recorded in Klg04, which would imply a recurrence rate of earthquakes of about 75 years. Such a high recurrence rate is improbable and we suspect that the reservoir age determined for the upper part of the cores is invalid during P4, perhaps because the stratification of the water body at the time of deposition of the sapropelic layer was different from the present one (Reimer and McCormac, 2002).

The P3 period is marked by a sedimentation rate at the Klg04 site half that at the Klg03 site. In addition, turbidite deposits are more frequent at the Klg03 site than at the Klg04 site. Finally, in Klg04 the end of period P3 is marked by an erosional event that occurred at AD385-864. These differences might be directly linked to the fact that less sediment was available during that time on the northern shelf and slopes than on the southern ones.

The P2 period is marked by a slight increase in sedimentation rate in Klg03 and by a large one in Klg04. The mean thickness of the turbidites increases and the two sites record exactly the same number of turbidites. The P3/P2 transition corresponds to a decrease in clay content and to an increase in silt recorded in all of the cores in the Marmara Sea (Figs. 3 and 4, and Drab et al. (2012)). It implies that sediment input to the Marmara Northern Margin was increasing even if watersheds around Istanbul were restricted and could not have been an important sediment sources (i.e. most of the sediment yield comes from rivers from the southern margin of the Marmara Sea (Smith et al., 1995)). This increase in sedimentation rate might be a consequence of the intensification of soil erosion and of agricultural development around Istanbul. This event might be related to the renewed development of Constantinople during the Ottoman period after 1453.

The most recent change in sedimentation rate is observed in Klg03 after 1894. The sedimentation rate increased to about 0.4 cm/yr due to the deposition of turbidite tA. This value is close to rates obtained during the 20^{th} century in lakes located on the southern part of the Marmara Sea and from sediment sampled from the Kocasu River, one of the major sediment sources for the Marmara Sea, and is characteristic of poor land use and deforestation (Kazanci et al., 2004). We interpret the increase in sedimentation rate occurring at the Klg03 site as linked to a marked increase in sediment input on the Marmara Southern shelf and slopes. The latter might be related to the dramatic shift in agricultural practices over the past century involving the replacement of working animals with machines. Due to the increase of sediment yield, mass failure related to far field earthquakes can occur as with the 1999 earthquake recorded in the Çınarcık Basin (Fig. 7).

Triggers of turbidites documented in Klg03 and Klg04

Considering the specific geomorphic setting of the Çınarcık Basin and the core locations (McHugh et al., 2006; Sarı and Çağatay, 2006), earthquakes and/or sediment loading are the only possible triggering mechanisms for turbidites in Klg03 and Klg04. Three distinct arguments lead us to consider that turbidites deposited in the studied cores are seismically generated. First, slope failure linked only to sediment loading on the northern slope of the Çınarcık Basin is questionable. The faulted margin of the basin in the vicinity of the Klg03 and Klg04 cores is too steep to accumulate a significant sedimentary load (Çağatay et al., 2012). In addition, sedimentary input on the Northern Shelf is restricted due to the very small watersheds draining the land to the north of the Çınarcık Basin. Cumulative Holocene sedimentation reaches a maximum of 2.5 m in the middle of the shelf and less than one meter in its southern part (Çağatay et al., 2009). Excess sedimentary loading on the edge of the shelf is thus unlikely.

Second, the turbidites we identified in Klg03 and Klg04 have sedimentological characteristics identical to the specific properties of earthquake-triggered turbidites in the Marmara

Sea and the Izmit Gulf studied by others (McHugh et al., 2006; Sarı and Çağatay, 2006; Beck et al., 2007; Drab et al., 2012; Çağatay et al., 2012) (see subsection Seismo-turbidite characteristics).

Finally, another test to determine if turbidites are seismically generated is to check the synchronicity of the documented events regionally (Goldfinger, 2011; Goldfinger et al., 2012; McCalpin, 1996). Our test rests upon the time correlation obtained to the dated reference core, Klg06, located in a different structural setting. Figure 6 shows that the turbidites in Klg04 core are systematically correlated to ones in Klg03. The Klg03 and Klg04 cores are however only separated by 3 km, a distance that might not be large enough to completely fulfill this synchronicity test. We thus looked at the C15 core (Sarı and Çağatay, 2006) located several kilometers from Klg03 (Fig. 1). Sarı and Çağatay (2006) documented quartz-rich seismoturbidites at 61 cm and 74 cm with uncalibrated ages of 1470±35 yr BP and 1890±35 yr BP. Independently of any age reservoir correction, the radiocarbon ages imply that the two turbidites correlate with events E2 and E3 in both Klg03 and Klg04 (Fig. A.2 in the appendices). In addition, the mineralogical characteristics of these instantaneous deposits are also similar to turbidites E2 and E3.

Based on their distinctive characteristics, large lateral extent and synchronicity, we conclude that the turbidites deposited simultaneously in Klg03 and Klg04 are earthquake triggered. The original mass failure would come from the Çınarcık Northern Slope (see subsection core correlation) and must be related to rupture of the fault running at the slope base. We thus infer that these seismoturbidites have been triggered by large earthquakes along the Northern Çınarcık Fault segment.

The Klg03 site is located on the Çınarcık Basin floor, where seismoturbidites from different sources can be deposited. The Basin is bounded to the north and south by the Çınarcık Segment and the Southern Segment, respectively; to the west by the Central Segment crossing the Central High; and to the east by the Izmit Segment (Fig. 1-a). A M>7 earthquake along one of these faults would destabilize broad parts of the bounding slopes and initiate a huge volume of sediment flows. Extensive flows (i.e., turbidites) can travel considerable distances across flat basin floors. We speculate that the turbidites present in Klg03 but not in Klg04 may have a seismic trigger but with a far field origin. The seismicity in the region is so high that earthquakes are the most likely trigger for slope failure. Indeed, the first turbidite recorded in Klg03, labeled tA, occurred very recently according to radionuclide data and can be attributed to the M=7.4 1999 earthquake (Fig. 7). A similar far-field turbidite was triggered in the Black Sea approximately at the same distance as the Çınarcık Basin (Yücel et al., 2010). The event has a particular sedimentological imprint with a non-erosive base associated with an increase in magnetic susceptibility and grain size.

Inferred rupture history for the Çınarcık Segment and adjacent segments

During the last 1500 years six synchronous earthquake-related turbidites were deposited simultaneously in a berm at the foot of the Çınarcık Fault and in the main depocenter of the Çınarcık Basin. A significant erosional event in Klg04, E5, correlated with a main basin turbidite in Klg03, also occurred. We infer that the obtained sedimentary record is related to widespread sedimentary failures along the slope and the edge of the northern shelf, induced by the rupture of the Çınarcık Fault. In the following section we will first compare the history of ruptures of the Çınarcık Fault with historical records. From the combination of the present data set and paleoseismological record (Table 1), a coherent history of ruptures can be reconstructed.

The OxCal chronology (Table 2) strongly suggests that the first four events are related to M>6.8 earthquakes occurring in 1894, in 1509, during the 14^{th} century (1296, 1353, 1344 or 1343) and in 989. Below event E4, Klg04 displays the erosional event E5 (AD399-AD867) that may have been induced by the AD740 historical earthquake. Finally, event E6 could be attributed to either the 437 or 407 earthquake. Due to limited time constraints at greater depth, we will focus our discussion only on events E1 to E6, which are corroborated with historical and paleoseismological data from previous studies. Potential geographical limits of past fault ruptures along the Çınarcık Fault are then inferred using other paleoseismological records.

The M=7.3 1894 earthquake (Ambraseys, 2002) affected a large area from Istanbul to Izmit (see isointensity curves from Eginitis (1894) in Ince (2011)). Ambraseys (2002) located the earthquake epicenter in the East of the Marmara Sea near the Hersek Peninsula. A significant tsunami in Bosphorus and Prince Islands (Yalçıner et al., 2002; Altınok et al., 2011) was associated with this earthquake. Using a modeling approach for the tsunami, Hebert et al. (2005) concluded that the 1894 earthquake source must have extended in the Çınarcık Basin, likely with a normal component. Pondard et al. (2007), using Coulomb stress failure modeling, also deduced that the 1894 earthquake broke the northern or southern bounding fault of the Çınarcık Basin. Klg03 and Klg04 both record the 1894 earthquake, implying that the northern Çınarcık Fault ruptured.

A westward propagating earthquake sequence, labeled Sequence 3 on Figure 11, transpired during the 18^{th} century, comprising four strong shocks in 1719, 1754, May 1766 and Aug 1766. The M=7.4 1719 and the M=6.8 1754 earthquakes occurred in the eastern part of the Marmara Sea (Ambraseys, 2002). There is widespread evidence of an 18^{th} century earthquake in paleoseismic trenches along the 1999 Düzce and Izmit earthquake ruptures (Rockwell et al., 2001; Sugai et al., 2001; Klinger et al., 2003; Rockwell et al., 2009; Fraser et al., 2010), but it is not possible to determine exactly which earthquake occurred at a particular spot within this time window. The Aug. 1766 earthquake occurred in the western part of the Marmara Sea, and paleoseismic trenches west of the Marmara Sea also reveal surface ruptures attributed to the 1659 (Ms=7.2) or to the Aug. 1766 (Ms=7.4) earthquakes (Rockwell et al., 2009; Meghraoui et al., 2012). The location of the M=7.1 May 1766 earthquake is strongly debated with Ambraseys (2002) inferring a location in the Çınarcık Basin and others (Pondard et al., 2007) in the Central Basin. The triggered tsunami induced damage in the Bosphorus (Yalçıner et al., 2002) and suggests a rupture in the Çınarcık Basin (Hebert et al., 2005). There are no apparent turbidites recorded during that period along the Çınarcık Fault, but Drab et al. (2012) documented seismoturbidites, probably related to the May and Aug. 1766 earthquakes, in the Tekirdağ and Central Basins. In addition, there is no surface rupture across the Hersek Delta during that period (Kozaci et al., 2010, 2011) and the sediment record in the Karamusel Basin (Çağatay et al., 2012) contains no distinctive identifying signal of these earthquakes. We thus favor the following scenario: the 1719 and 1754 earthquakes occurred East of the Hersek Peninsula, the May 1766 earthquake broke the Central Fault and the 1659 and Aug. 1766 earthquakes ruptured the Ganos and Tekirdağ Faults. This scenario is still compatible with earthquake damages (Ambraseys, 2002). However, it is not possible to exclude that the May 1766 ruptured a fault along the southern edge of the Çınarcık Basin, a scenario more compatible with Coulomb stress analysis of (Pondard et al., 2007).

The 1509 earthquake caused heavy damages on both sides of Istanbul implying an epicenter location at the boundary between the Çınarcık and the Central Faults (Ambraseys, 2002). The earthquake triggered a large tsunami (6 m run up; Ambraseys and Finkel (1991); Yalçıner et al. (2002)) attributed to the rupture of the narck Fault (Hebert et al., 2005). Our records from the Klg03 and Klg04 cores are compatible with this scenario. Paleoseismic data further east also suggests an NAF rupture at that time, with the most recent surface rupture across the Hersek Delta (Kozaci et al., 2010, 2011) attributed to the 1509 earthquake. The earthquake rupture is confirmed further east in paleoseismic trenches (Klinger et al., 2003) and recorded in cores just west of Hersek (McHugh et al., 2006), in the Hersek Lagoon (Bertrand et al., 2011), and in the Karamusel Bay (Çağatay et al., 2012). The inferred 100 km-long rupture would be compatible with the estimate 70±30 km long rupture estimated in Ambraseys (2001).

During the 13^{th} and 14^{th} centuries there was a sequence of earthquakes (Sequence 2 on Fig. 11) in the Marmara region in 1296 (Ms=7), 1343 (Ms=7), 1344 (Ms=6.9), 1354 (Ms=7.4). The 1296 earthquake occurred in the east of the Çınarcık Basin (Ambraseys, 2002) and was documented in the Karamusel Basin (Çağatay et al., 2012). The 1343 and 1354 earthquakes occurred in the western part of the Marmara Sea and were confirmed in paleoseismic trenches (Rockwell et al., 2001, 2009; Meghraoui et al., 2012). McHugh et al. (2006) documented a seismoturbidite in the Central Basin attributed to the 1343 earthquake. Based on historical sources, the 1344 earthquake has been located in the central part of the Marmara Sea (Ambraseys, 2002). It was associated with a tsunami that caused significant damage in Istanbul and inundated the Bosphorus 2000 m away (Altınok et al., 2011). A 1.2 m tectonic uplift of the Hersek Peninsula (Özaksoy et al., 2010) also occurred during that time period. Finally, we documented one of these events in our cores. We thus conclude that the 1344 earthquake ruptured the Çınarcık Fault as it is the only event that triggered a tsunami in Istanbul (Hebert et al., 2005). In that case, the 1354 and 1343 earthquakes would have occurred on the Central-Tekirdağ-Ganos Faults and the 1296 earthquake on the Izmit Fault.

The M=7.2 989 earthquake (Sequence 1) was located in the Çınarcık Basin (Ambraseys, 2002) and was associated with a damaging tsunami in Istanbul (Altınok et al., 2011). The event was also recorded in the Hersek Lagoon (Bertrand et al., 2011), but not in the Karamusel Basin (Çağatay et al., 2012). Because we record a turbidite at that time (E4), we conclude that the 989 earthquake ruptured the Çınarcık Fault and may have extended to the Hersek Peninsula.

The Event Erosion is correlated with turbidite E5 in Klg03 and is dated between AD399-

AD867. This age range encompasses the age of the event E6. The most probable age range for E5 may thus be AD512-AD867. The largest earthquake within this age range is the M=7.1 740 earthquake. Ambraseys (2002) located the epicenter of this earthquake in the Çınarcık Basin. The earthquake was associated with 1) a large tsunami (Altınok et al., 2011) affecting Istanbul the Izmit Area; and 2) an atypical subsidence in the Hersek Peninsula of about 2 m (Bertrand et al., 2011). This earthquake was also documented in the Central Basin (McHugh et al., 2006) and in the Izmit Bay (Çağatay et al., 2012). We thus conclude that the 740 earthquake may be associated with the Erosional Event, E5, recorded in Klg04.

Finally, Event E6 occurred between AD20 and AD512. According to historical reports, Ambraseys (2002) locate two earthquakes during that time lag (the M=6.6 407 and the M=6.8 437) while Guidoboni et al. (1994) also locate the M=7.2 447 and M=7.3 478 earthquake in Istanbul Area. Only the 407, 447 and 478 earthquakes were associated with a tsunami invading Istanbul (Altınok et al., 2011). According to historical reports, the 478 earthquake was associated with a stronger tsunami. E6 may be related to one of these earthquakes and perhaps more likely with the M=7.3 478 earthquake. It is also consistent with the average recurrence interval calculated for the segment. Nevertheless, the lack of information from other studies does not allow us to further discuss the location of this earthquake.

Since the 9^{th} century, three complete sequences have released stresses along the NAF (Fig. 11). The present seismic cycle is incomplete, with a seismic gap along Central Fault and Çınarcık Fault (Hubert-Ferrari et al., 2000; Parsons et al., 2000). Figure 11 also shows that no clear rupture propagation direction prevails and highlights the importance of the 30° bend located at the western extremity of the Çınarcık Fault (Carton et al., 2007), which may act as a permanent seismic barrier. In addition, some ruptures along the Çınarcık Fault are out of sequence as in the 1894 earthquake. The latter may be linked to the stress shadow induced by the May 1766 rupture of a secondary normal fault segment. The stress shadow may have delayed rupture along the Çınarcık Segment by 130 years. Finally, segments seem to have similar activity, implying no specific creep, with possible exception on the Central Fault (Drab et al., 2012). Further paleoseismic studies in the Central Basin are required to confirm this hypothesis, which has strong implications for hazard assessment in the Istanbul area, both in terms of the recurrence rate and the maximum magnitude of earthquakes along this segment.

Conclusion

We have applied the concepts of sub-aquatic paleoseismology to two sediment cores located 20 km south to Istanbul in the Çınarcık Basin (Marmara Sea) to assess past fault rupture history along the Çınarcık Segment of the North Anatolian Fault. Historical seismicity suggests that this segment has ruptured in M>7 earthquakes. The cores are composed of about 50-60% of turbidites. Based on their distinctive sedimentological characteristics, their geographical extent, synchronicity and by the exclusion of other triggering mechanisms, the studied turbidites are concluded to be earthquake-triggered. Core Klg04, located on the berm in the northern fault margin of the basin, likely records earthquakes rupturing the Çınarcık Fault while Klg03 may record earthquakes occurring on other faults and highlights the different sensitivity of both sites to earthquakes. We estimated the timing of the first six sedimentary events using radiocarbon dating, radionuclides and paleomagnetism measurements. Radiocarbon dating was calibrated using OxCal software and was corrected for marine reservoirs with a local reservoir correction of 400±50 years, implying that the total reservoir age in the Sea of Marmara is about 800 years for the last 2000 years. The first earthquake-related turbidite recorded in the cores corresponds to the 1894 earthquake. Event E2 occurred between AD1288-1664 and is probably related to the 1509 historical earthquake. Event E3 was dated AD1178-1399 and was likely generated by the 1344 earthquake. Event E4, which occurred between AD710-1164, was triggered by the 989 earthquake. The erosional event, E5, may be related to the 740 earthquake. Finally Event E6 (AD20-AD512) may be related to the 478 earthquake. The integration of our results enables us to propose a coherent scenario of past ruptures along the Çınarcık Fault, which can be used for seismic hazard assessment. Indeed, our observations help relocate some earthquake for which the rupture segment is still under debate. We suggest that the 1766 earthquake did not occur along the Çınarcık Fault, but that the 1344 earthquake was likely related to its activation. To obtain a better understanding of segment ruptures, a strengthened age model of sediment deposition in the Marmara Sea will require the acquisition of additional cores along the fault and in the basin.

Data and resources

All historical earthquakes data used in this paper came from published sources listed in the references. Maps were made using ArcGis 9.3. Plots were obtained by using Excel.

Acknowledgments

We first would like to thank Rolando Armijo who was the chief scientist of the Marmarascarps mission in 2002 from which we studied the two cores. We acknowledge Jean Luc Schneider for his help in core logging. We are grateful to Isabelle Billy, Joel Saint-Paul and Olivier Ther for core sampling, realization of X-ray scanner imagery and XRF data acquisition. We would like to thank Elisabeth Michel and Elisabeth Tellier for their help on foraminifers extraction. We are also grateful to Catherine Kissel who allowed us finishing our paleomagnetic measurements when the magnetometer of the IPGP was not available.

Radiocarbon dating was supported by the CNRS-INSU Artemis program and done in the Artemis LMC14 laboratory as well as by the Crdit chercheur du fond national pour la Recherche Scientifique Belge under the project SEISMARM. The program CNRS/FRS-FNRS CGRI supported grain size and XRD data acquisition in Liège (Belgium) and the ENS, UMR8538 provided additional financial support for data acquisition. We would like to thank Giuseppe Siani for fruitful discussions. Finally, we would like to thank Carl Brenner for improving the English grammar and expression.

References

Altınok, Y., Alpar, B., Özer, N., and Aykurt, H. (2011). Revision of the tsunami catalogue affecting turkish coasts and surrounding regions. *Natural Hazards and Earth System Sciences*, 11(2):273–291.

Ambraseys, N. (2001). The earthquake of 1509 in the Sea of Marmara, Turkey, revisited. *Bulletin of the Seismological Society of America*, 91(6):1397–1416.

Ambraseys, N. (2002). The seismic activity of the Marmara Sea region over the last 2000 years. *Bulletin of the Seismological Society of America*, 92(1):1–18.

Ambraseys, N. and Finkel, C. (1991). Long-term seismicity of Istanbul and of the Marmara Sea region. *Terra Nova*, 3(5):527–539.

Ambraseys, N. (2009). *Earthquakes in the Mediterranean and Middle East*. Cambridge University Press New York.

Armijo, R., Meyer, B., Navarro, S., King, G., and Barka, A. (2002). Asymmetric slip partitioning in the Sea of Marmara pull-apart: a clue to propagation processes of the North Anatolian Fault? *Terra Nova*, 14(2):80–86.

Armijo, R., Pondard, N., Meyer, B., Uçarkuş, G., de Lepinay, B., Malavieille, J., Dominguez, S., Gutscher, M., Schmidt, S., Beck, C., Çağatay, N., Çakır, Z., Imren, C., Eriş, K., Natalin, B., Ozalaybey, S., Tolun, L., Lefevre, I., Seeber, L., Gasperini, L., Rangin, C., Emre, O., and Sarikavak, K. (2005). Submarine fault scarps in the Sea of Marmara pull-apart (North Anatolian Fault): Implications for seismic hazard in Istanbul. *Geochemistry, Geophysics, Geosystems*, 6:1–29.

Bahr, A., Lamy, F., Arz, H., Kuhlmann, H., and Wefer, G. (2005). Late glacial to Holocene climate and sedimentation history in the NW Black Sea. *Marine Geology*, 214(4):309–322.

Barka, A. and Kadinsky-Cade, K. (1988). Strike-slip fault geometry in Turkey and its influence on earthquake activity. *Tectonics*, 7(3):663–684.

Beck, C., Mercier de Lépinay, B., Schneider, J., Cremer, M., Çağatay, N., Wendenbaum, E., Boutareaud, S., Ménot, G., Schmidt, S., Weber, O., Eriş, K., Armijo, R., Meyer, B., Pondard, N., Gutscher, M., the Marmacore cruise party, Turon, J., Labeyrie, L., Cortijo, E., Gallet, Y., Bouquerel, H., Görür, N., Gervais, A., Castera, M., Londeix, L., de Resseguier, A., and Jaouen, A. (2007). Late quaternary co-seismic sedimentation in the Sea of Marmara's deep basins. *Sedimentary Geology*, 199(1−2):65–89.

Bertrand, S., Charlet, F., Chapron, E., Fagel, N., and De Batist, M. (2008). Reconstruction of the holocene seismotectonic activity of the southern andes from seismites recorded in lago Icalma, Chile, 39 s. *Palaeogeography, Palaeoclimatology, Palaeoecology*, 259(2-3):301–322.

Bertrand, S., Doner, L., Ön, S., Sancar, U., Schudack, U., Mischke, S., Çagatay, M., and Leroy, S. (2011). Sedimentary record of coseismic subsidence in hersek coastal lagoon (Izmit Bay, Turkey) and the late holocene activity of the north anatolian fault. *Geochemistry, Geophysics, Geosystems*, 12(6):Q06002.

Bronk Ramsey, C. (2007). Oxcal program, v. 4.0. *Radiocarbon Accelerator Unit, University of Oxford, UK.*

Bulut, F. and Aktar, M. (2007). Accurate relocation of izmit earthquake (mw = 7.4, 1999) aftershocks in Çınarcık basin using double difference method. *Geophysical Research Letters*, 34(10):L10307.

Butler, R. (1992). *Paleomagnetism: magnetic domains to geologic terranes.* Blackwell Scientific Publications Boston, MA.

Calvert, S. (1990). Geochemistry and origin of the holocene sapropel in the Black Sea. *Facets of modern biogeochemistry: Berlin, Springer-Verlag*, pages 326–352.

Campos, C., Beck, C., Crouzet, C., Demory, F., Van Welden, A., and Eris, K. (2013). Deciphering hemipelagites from homogenites through anisotropy of magnetic susceptibility. paleoseismic implications (sea of marmara and gulf of corinth). *Sedimentary Geology*, 292(0):1–14.

Carton, H., Singh, S. C., Hirn, A., Bazin, S., de Voogd, B., Vigner, A., Ricolleau, A., Cetin, S., Ocakoglu, N., Karakoc, F., and Sevilgen, V. (2007). Seismic imaging of the three-dimensional architecture of the Çınarcık Basin along the North Anatolian Fault. *Journal of Geophysical Research-Solid Earth*, 112(B6):B06101.

Çağatay, M., Algan, O., Sakinç, M., Eastoe, M., Egesel, L., Balkis, N., Ongan, D., and Caner, H. (1999). A mid-late holocene sapropelic sediment unit from the southern Marmara Sea shelf and its palaeoceanographic significance. *Quaternary Science Reviews*, 18(4-5):531–540.

Çağatay, M., Erel, L., Bellucci, L., Polonia, A., Gasperini, L., Eriş, K., Sancar, U., Biltekin, D., Uçarkuş, G., Ulgen, U., and Damcı, E. (2012). Sedimentary earthquake records in the Izmit Gulf, Sea of Marmara, turkey. *Sedimentary Geology*, 282(0):347–359.

Çağatay, M., Eriş, K., Ryan, W., Sancar, U., Polonia, A., Akcer, S., Biltekin, D., Gasperini, L., Görür, N., Lericolais, G., and Bard, E. (2009). Late Pleistocene-Holocene evolution of the northern shelf of the Sea of Marmara. *Marine Geology*, 265(3-4):87–100.

Çağatay, M., Görür, N., Algan, O., Eastoe, C., Tchapalyga, A., Ongan, D., Kuhn, T., and Kuşcu, I. (2000). Late Glacial-Holocene palaeoceanography of the Sea of Marmara: timing of connections with the Mediterranean and the Black Seas. *Marine Geology*, 167(3-4):191–206.

Çağatay, M., Özcan, M., and Güngör, E. (2004). Pore-water and sediment geochemistry in the Marmara Sea (Turkey): early diagenesis and diffusive fluxes. *Geochemistry: Exploration, environment, analysis*, 4(3):213–225.

Cogné, J. (2003). Paleomac: a macintoshtm application for treating paleomagnetic data and making plate reconstructions. *Geochemistry, Geophysics, Geosystems*, 4(1):1007.

Cramp, A. and O'Sullivan, G. (1999). Neogene sapropels in the Mediterranean: a review. *Marine Geology*, 153(1-4):11–28.

Cuven, S., Francus, P., and Lamoureux, S. (2010). Estimation of grain size variability with micro x-ray fluorescence in laminated lacustrine sediments, cape bounty, canadian high arctic. *Journal of Paleolimnology*, 44(3):803–817.

Drab, L. (2012). *Étude multidisciplinaire le long de la Faille Nord Anatolienne, Turquie :Paléosismologie marine et paléomagnétisme en Mer de Marmara; Étude gomor-*

phologique du décalage de la rivière Kızılırmak par utilisation des isotopes cosmogéniques. PhD thesis, Ecole Normale supérieure, Université Paris Sud XI.

Drab, L., Hubert, A., Schmidt, S., and Martinez, P. (2012). The earthquake sedimentary record in the western part of the sea of Marmara, Turkey. *Natural Hazards & Earth System Sciences*, 12(4):1235–1254.

Eastwood, W., Roberts, N., and Lamb, H. (1998). Palaeoecological and archaeological evidence for human occupance in southwest Turkey: the Beyşehir occupation phase. *Anatolian Studies*, 48:69–86.

Eginitis, M. (1894). Earthquake report. Technical report, Prime Minister's Archive.

Folk, R. (1968). *Petrology of sedimentary rocks*. Hemphill's Austin, Texas.

Fraser, J., Vanneste, K., and Hubert-Ferrari, A. (2010). Recent behavior of the North Anatolian Fault: Insights from an integrated paleoseismological data set. *Journal of Geophysical Research*, 115(B9):B09316.

Goldfinger, C. (2011). The record of large turbidites and their relevance to the history of earthquakes. *Annual Review of Marine Science*, 3(1).

Goldfinger, C., Grijalva, K., Bürgmann, R., Morey, A., Johnson, J., Nelson, C., Gutiérrez-Pastor, J., Ericsson, A., Karabanov, E., Chaytor, J., Patton, J., and Gracia, E. (2008). Late holocene rupture of the northern San Sndreas fault and possible stress linkage to the cascadia subduction zone. *Bulletin of the Seismological Society of America*, 98(2):861–889.

Goldfinger, C., Nelson, C., Morey, A., Johnson, J., Gutierrez-Pastor, J., Eriksson, A., Karabanov, E., Patton, J., Gràcia, E., Enkin, R., et al. (2012). *Turbidite event history:*

Methods and implications for Holocene paleoseismicity of the Cascadia subduction zone. US Department of the Interior, US Geological Survey.

Gorsline, D., De Diego, T., and Nava-Sanchez, E. (2000). Seismically triggered turbidites in small margin basins: Alfonso basin, western gulf of California and Santa Monica basin, California borderland. *Sedimentary Geology*, 135(1-4):21–35.

Gracia, E., Vizcaino, A., Escutia, C., Asioli, A., Rodes, A., Pallas, R., Garcia-Orellana, J., Lebreiro, S., and Goldfinger, C. (2010). Holocene earthquake record offshore portugal (sw iberia): testing turbidite paleoseismology in a slow-convergence margin. *Quaternary Science Reviews*, 29(910):1156–1172.

Guidoboni, E., Comastri, A., Traina, G., Phillips, B., and nazionale di geofisica (Italie), I. (1994). *Catalogue of Ancient Earthquakes in the Mediterranean Area up to the 10th Century*. Istituto nazionale di geofisica.

Hebert, H., Schindele, F., Altınok, Y., Alpar, B., and Gazioglu, C. (2005). Tsunami hazard in the Marmara Sea (Turkey): a numerical approach to discuss active faulting and impact on the Istanbul coastal areas. *Marine Geology*, 215(1-2):23–43.

Hubert-Ferrari, A., Barka, A., Jacques, E., Nalbant, S., Meyer, B., Armijo, R., Tapponnier, P., and King, G. (2000). Seismic hazard in the Marmara Sea region following the 17 August 1999 Izmit earthquake. *Nature*, 404(6775):269–273.

Ince, G. (2011). The relationship between the performance of soil conditions and damage following an earthquake: a case study in istanbul, turkey. *Natural Hazards and Earth System Sciences*, 11:1745–1758.

Kagan, E., Stein, M., Agnon, A., and Ramsey, C. (2010). Paleoearthquakes as anchor points in bayesian radiocarbon deposition models: A case study from the dead sea. *Radiocarbon*, 52(3):1018–1026.

Kazanci, N., Leroy, S., Ileri, O., Emre, O., Kibar, M., and Oncel, S. (2004). Late holocene erosion in NW Anatolia from sediments of lake Manyas, lake Ulubat and the southern shelf of the Marmara sea, Turkey. *Catena*, 57(3):277–308.

Kirschvink, J. (1980). The least-squares line and plane and the analysis of palaeomagnetic data. *Geophysical Journal of the Royal Astronomical Society*, 62(3):699–718.

Klinger, Y., Sieh, K., Altunel, E., Akoglu, A., Barka, A., Dawson, T., Gonzalez, T., Meltzner, A., and Rockwell, T. (2003). Paleoseismic evidence of characteristic slip on the western segment of the North Anatolian fault, Turkey. *Bulletin of the Seismological Society of America*, 93(6):2317–2332.

Korte, M. and Constable, C. (2011). Improving geomagnetic field reconstructions for 0-3ka. *Physics of the Earth and Planetary Interiors*, 188(3):247–259.

Kozaci, O., Altunel, E., Clahan, K., Yonlu, O., Sundermann, S., Lettis, W., Turner, J., Altekruse, J., Gumus, I., and Lindvall, S. (2010). A late holocene slip rate of the North Anatolian Fault, Hersek Peninsula, Izmit Bay, Turkey. In *AGU Fall Meeting Abstracts*, volume 1, page 2236.

Kozaci, Ö., Altunel, E., Lindvall, S., Brankman, C., and Lettis, W. (2011). The north anatolian fault on Hersek Peninsula, Turkey: Its geometry and implications on the 1999 Izmit earthquake rupture propagation. *Turkish Journal of Earth Science*, 20.

Larrasoaña, J., Roberts, A., Stoner, J., Richter, C., and Wehausen, R. (2003). A new proxy for bottom-water ventilation in the eastern mediterranean based on diagenetically controlled magnetic properties of sapropel-bearing sediments. *Palaeogeography, Palaeoclimatology, Palaeoecology*, 190:221–242.

Le Pichon, X., Sengör, A., Demirbag, E., Rangin, C., Imren, C., Armijo, R., Görür, N., Çagatay, N., Mercier de Lepinay, B., Meyer, B., SaatçIlar, R., and Tok, B. (2001). The active main Marmara Fault. *Earth and Planetary Science Letters*, 192(4):595–616.

Leroy, S., Kazancı, N., leri, O., Kibar, M., Emre, O., McGee, E., and Griffiths, H. (2002). Abrupt environmental changes within a late Holocene lacustrine sequence south of the Marmara Sea (Lake Manyas, NW Turkey): possible links with seismic events. *Marine Geology*, 190(1-2):531–552.

Lienkaemper, J. and Ramsey, C. (2009). Oxcal: Versatile tool for developing paleoearthquake chronologies: A primer. *Seismological Research Letters*, 80(3):431–434.

Lima, A., Hubeny, J., Reddy, C. M., King, J., Hughen, K., and Eglinton, T. (2005). High-resolution historical records from pettaquamscutt river basin sediments: 1. 210 pb and varve chronologies validate record of 137 cs released by the chernobyl accident. *Geochimica et Cosmochimica Acta*, 69(7):1803–1812.

Masson, D., Arzola, R., Wynn, J., Hunt, E., and P., W. (2011). Seismic triggering of landslides and turbidity currents offshore portugal. *Geochemistry, Geophysics, Geosystems*, 12(12):Q12011.

McCalpin, J. (1996). *Paleoseismology*. Academic Press.

McClusky, S., Reilinger, R., Mahmoud, S., Ben Sari, D., and Tealeb, A. (2003). GPS constraints on Africa (Nubia) and Arabia plate motions. *Geophysical Journal International*, 155(1):126–138.

McHugh, C., Seeber, L., Braudy, N., Cormier, M., Davis, M., Diebold, J., Dieudonne, N., Douilly, R., Gulick, S., Hornbach, M., et al. (2011). Offshore sedimentary effects of the 12 january 2010 Haiti earthquake. *Geology*, 39(8):723–726.

McHugh, C., Seeber, L., Cormier, M., Dutton, J., Çağatay, N., Polonia, A., Ryan, W., and Gorur, N. (2006). Submarine earthquake geology along the North Anatolia Fault in the Marmara Sea, Turkey: A model for transform basin sedimentation. *Earth and Planetary Science Letters*, 248(3-4):661–684.

Meghraoui, M., Aksoy, M., Akyüz, H., Ferry, M., Dikbaş, A., and Altunel, E. (2012). Paleoseismology of the north anatolian fault at güzelköy (Ganos Segment, Turkey): Size and recurrence time of earthquake ruptures west of the Sea of Marmara. *Geochemistry, Geophysics, Geosystems*, 13(4):Q04005.

Mudie, P., Marret, F., Aksu, A., Hiscott, R., and Gillespie, H. (2007). Palynological evidence for climatic change, anthropogenic activity and outflow of black sea water during the late pleistocene and holocene: Centennial- to decadal-scale records from the Black and Marmara Seas. *Quaternary International*, 167-168:73–90.

Mudie, P., Rochon, A., and Aksu, A. (2002). Pollen stratigraphy of Late Quaternary cores from Marmara Sea: land-sea correlation and paleoclimatic history. *Marine Geology*, 190(1-2):233–260.

Nakajima, T. and Kanai, Y. (2000). Sedimentary features of seismoturbidites triggered by the 1983 and older historical earthquakes in the eastern margin of the Japan Sea. *Sedimentary Geology*, 135(1-4):1–19.

Özaksoy, V., Emre, Ö., Yıldırım, C., Doğan, A., Özalp, S., and Tokay, F. (2010). Sedimentary record of late holocene seismicity and uplift of Hersek restraining bend along the North Anatolian Fault in the gulf of Izmit. *Tectonophysics*, 487(1):33–45.

Palike, H., Shackleton, N., and Rohl, U. (2001). Astronomical forcing in late eocene marine sediments. *Earth and Planetary Science Letters*, 193(3-4):589–602.

Parsons, T. (2004). Recalculated probability of M>7 earthquakes beneath the Sea of Marmara, Turkey. *Journal of Geophysical Research*, 109(B5):B05304.

Parsons, T., Toda, S., Stein, R., Barka, A., and Dieterich, J. (2000). Heightened odds of large earthquakes near Istanbul: an interaction-based probability calculation. *Science*, 288(5466):661–665.

Pondard, N., Armijo, R., King, G., Meyer, B., and Flerit, F. (2007). Fault interactions in the Sea of Marmara pull-apart (North Anatolian Fault): earthquake clustering and propagating earthquake sequences. *Geophysical Journal International*, 171(3):1185–1197.

Reilinger, R., McClusky, S., Vernant, P., Lawrence, S., Ergintav, S., Cakmak, R., Ozener, H., Kadirov, F., Guliev, I., Stepanyan, R., et al. (2006). GPS constraints on continental deformation in the Africa-Arabia-Eurasia continental collision zone and implications for the dynamics of plate interactions. *Journal of Geophysical Research*, 111(B5):B05411.

Reimer, P., Bard, E., Bayliss, A., Beck, J., Blackwell, P., Ramsey, C., B, C., Cheng, H., Edwards, R., Friedrich, M., Grootes, P., Guilderson, T., Haflidason, H., Hajdas, I., Hatte, C., Heaton, T., Hoffmann, D., Hogg, A., Hughen, K., Kaiser, K., Kromer, B., Manning, S., Niu, M., Reimer, R., Richards, D., Scott, E., Southon, J., Staff, R., Turney, C., and van der Plicht, J. (2013). Intcal13 and marine13 radiocarbon age calibration curves $0-50{,}000$ years cal bp. *Radiocarbon*, 55(4):1869–1887.

Reimer, P. and McCormac, F. (2002). Marine radiocarbon reservoir corrections for the Mediterranean and Aegean Seas. *Radiocarbon*, 44(1):159–166.

Robbins, J. (1978). Geochemical and geophysical applications of radioactive lead. *The biogeochemistry of lead in the environment*, 1:285–337.

Rockwell, T., Barka, A., Dawson, T., Akyuz, S., and Thorup, K. (2001). Paleoseismology of the Gazikoy-Saros segment of the North Anatolia Fault, northwestern Turkey: Comparison of the historical and paleoseismic records, implications of regional seismic hazard, and models of earthquake recurrence. *Journal of Seismology*, 5(3):433–448.

Rockwell, T., Ragona, D., Seitz, G., Langridge, R., Aksoy, M., Uçarkuş, G., Ferry, M., Meltzner, A., Klinger, Y., Meghraoui, M., et al. (2009). Palaeoseismology of the North Anatolian Fault near the Marmara Sea: implications for fault segmentation and seismic hazard. *Geological Society, London, Special Publications*, 316(1):31–54.

Rohling, E. and Hilgen, F. (1991). The eastern mediterranean climate at times of sapropel formation: a review. *Geologie en Mijnbouw*, 70(3):253–264.

Sarı, E. and Çağatay, M. (2006). Turbidites and their association with past earthquakes in the deep Çınarcık Basin of the Marmara Sea. *Geo-Marine Letters*, 26(2):69–76.

Schmidt, S., Howa, H., Mouret, A., Lombard, F., Anschutz, P., and Labeyrie, L. (2009). Particle fluxes and recent sediment accumulation on the aquitanian margin of bay of biscay. *Continental Shelf Research*, 29(8):1044–1052.

Sengör, A., Tüysüz, O., Imren, C., Sakinç, M., Eyidogan, H., Görür, N., Le Pichon, X., and Rangin, C. (2005). The North Anatolian fault: A new look. *Annu. Rev. Earth Planet. Sci.*, 33:37–112.

Shiki, T., Kumon, F., Inouchi, Y., Kontani, Y., Sakamoto, T., Tateishi, M., Matsubara, H., and Fukuyama, K. (2000). Sedimentary features of the seismo-turbidites, lake biwa, japan. *Sedimentary Geology*, 135(1-4):37–50.

Siani, G., Paterne, M., Arnold, M., Bard, E., Metivier, B., Tisnerat, N., and Bassinot, F. (2000). Radiocarbon reservoir ages in the mediterranean sea and black sea. *Radiocarbon*, 42(2):271–280.

Siani, G., Paterne, M., Michel, E., Sulpizio, R., Sbrana, A., Arnold, M., and Haddad, G. (2001). Mediterranean sea surface radiocarbon reservoir age changes since the last glacial maximum. *Science*, 294(5548):1917–1920.

Smith, A., Taymaz, T., Oktay, F., Yüce, H., Alpar, B., Başaran, H., Jackson, J., Kara, S., and Şimşek, M. (1995). High-resolution seismic profiling in the sea of marmara (northwest turkey): Late quaternary sedimentation and sea-level changes. *Geological Society of America Bulletin*, 107(8):923–936.

Sperazza, M., Moore, J., and Hendrix, M. (2004). High-resolution particle size analysis of naturally occurring very fine-grained sediment through laser diffractometry. *Journal of Sedimentary Research*, 74(5):736–743.

Stuiver, M., Pearson, G. W., and Braziunas, T. F. (1986). Radiocarbon age calibration of marine samples back to 9000 cal yr bp. *Radiocarbon*, 28(2B):980–1021.

Sugai, T., Awata, Y., Toda, S., Emre, O., Dogan, A., Ozalp, S., Haraguchi, T., Kinoshita, H., Takada, K., and Yamaguchi, M. (2001). Paleoseismic investigation of the 1999 Düzce earthquake fault at Lake Efteni, North Anatolian fault system, Turkey. *Annual Report on Active Fault and Paleoearthquake Researches*, pages 339–351.

Tauxe, L. (2010). *Essentials of Paleomagnetism*. University of California Press.

Tauxe, L. and Kent, D. V. (1984). Properties of a detrital remanence carried by haematite from study of modern river deposits and laboratory redeposition experiments. *Geophysical Journal of the Royal Astronomical Society*, 76(3):543–561.

Tema, E. and Kondopoulou, D. (2011). Secular variation of the earth's magnetic field in the balkan region during the last eight millennia based on archaeomagnetic data. *Geophysical Journal International*, 186(2):603–614.

Tolun, L., Çağatay, M., and Carrigan, W. (2002). Organic geochemistry and origin of Late Glacial-Holocene sapropelic layers and associated sediments in Marmara Sea. *Marine Geology*, 190(1-2):47–60.

Uçarkuş, G. (2010). *Active faulting and earthquake scarps along the North Anatolian Fault in the Seo of Marmara.* PhD thesis, Istanbul Technical University.

van Welden, A., Beck, C., Reyss, J., Bushati, S., Koci, R., Jouanne, F., and Mugnier, J. (2008). The last 500 year of sedimentation in shkodra lake (albania/montenegro): paleoenvironmental evolution and potential for paleoseismicity studies. *Journal of Paleolimnology*, 40(2):619–633.

Vidal, L., Menot, G., Joly, C., Bruneton, H., Rostek, F., Çağatay, M. N., Major, C., and Bard, E. (2010). Hydrology in the Sea of Marmara during the last 23 ka: Implications for timing of Black Sea connections and sapropel deposition. *Paleoceanography*, 25(1):PA1205.

Vlag, P., Kruiver, P., and Dekkers, M. (2004). Evaluating climate change by multivariate statistical techniques on magnetic and chemical properties of marine sediments (azores region). *Palaeogeography, Palaeoclimatology, Palaeoecology*, 212(1-2):23–44.

Walling, D. (2006). Human impact on landocean sediment transfer by the world's rivers. *Geomorphology*, 79(34):192–216.

Yalçıner, A., Alpar, B., Altınok, Y., Özbay, İ., and Imamura, F. (2002). Tsunamis in the sea of marmara: Historical documents for the past, models for the future. *Marine Geology*, 190(1):445–463.

Yücel, M., Luther, G., and Moore, W. (2010). Earthquake-induced turbidite deposition as a previously unrecognized sink for hydrogen sulfide in the black sea sediments. *Marine Chemistry*, 121(1):176–186.

Author's affiliation

Laureen Drab: Ecole Normale Suprieure, 24 rue Lhomond 75231 Paris Cedex 05 France

now at : Lamont Doherty Earth Observatory, Columbia University, 61 Route 9W Palisades, NY, 10964 USA

Aurélia Hubert-Ferrari: Département de Géographie- Université de Liège- Allée du 6 aout, 2, Bat. B11- Sart Tilman B 4000- Liège - Belgique

Sabine Schmidt: UMR 5805 EPOC- Site de Talence-Université Bordeaux 1- Avenue des Facultés-33405 Talence Cedex- France

Philippe Martinez: UMR 5805 EPOC- Site de Talence-Université Bordeaux 1- Avenue des Facultés-33405 Talence Cedex- France

Julie Carlut: IPGP- 1, rue Jussieu- 75238 Paris Cedex 05- France

Meriam El Ouahabi: Département de Géographie- Université de Liège- Allée du 6 aout, 2, Bat. B11- Sart Tilman B 4000- Liège - Belgique

Captions

Figure 1: a/ General tectonic map of the Marmara Sea, crossed by the North Anatolian Fault (NAF). Basins, highs and main segments of the fault are indicated from the west to the east with different lines and their names are given in the gray box to the right. The study area is depicted with a box. Historical earthquakes located by Ambraseys (2002) are represented with a white dot. b/ Global geodynamic context of the Anatolian Plate with GPS velocities from Reilinger et al. (2006). The location of the Marmara Sea is indicated with a box. c/ Map of Çınarcık Basin and location of the two studied cores (Klg03 (40°47.98N; 28°59.55E) and Klg04 (40°48.60N; 29°00.73E) represented with a white cross) with respect to the Çınarcık Fault segment. Arrows show sediment paths for turbidite deposits (Altınok et al., 2011). The line crossing the two cores represent the path topographic profile presented in d/. Black crosses represent the location of other published cores discussed in the study. d/ Topographic profile of the northern part of the Çınarcık Basin. The profile starts at Klg03 core location.

Figure 2: Stratigraphic obtained combining X-ray imagery, particle size, magnetic susceptibility data, Mn and Zr standardized intensities. Major erosive deposited turbidites are labelled, beginning with 1 at the top of the core. Sandy beds are depicted in black, intermediate silty beds in gray, upper clay-rich beds in light gray and hemipelagic sedimentation in white. Sand layers name is given when the percentage of sand is greater than the background percentage. Description of the turbidites seen in the X-ray radiographs is also given with different symbols on the right side of the core log. Turbidites without an erosive base are labelled with a letter.

Figure 3: Stratigraphic obtained combining X-ray imagery, particle size, magnetic susceptibility data, Mn and Zr standardized intensities. Major erosive deposited turbidites are labelled, beginning with 1 at the top of the core. Sandy beds are depicted in black, intermediate silty beds in gray, upper clay-rich beds in light gray and hemipelagic sedimentation in white. Sand layers name is given when the percentage of sand is greater than the background percentage. Description of the turbidites seen in the X-ray radiographs is also given with different symbols on the right side of the core log.

Figure 4: Typical examples of turbidites: granulometric and geochemical (Ca/Ti, Mn, Zr and MS) signatures. Turbidites are composed of a basal sand layer, an upper silt layer with frequent laminations and an upper light gray clayey layer. a/ X-ray imagery, granulometry and geochemical profiles of turbidite e4 at 120 cm depth in Klg03. b/ X-ray imagery, granulometry and geochemical profiles of turbidite e2 at 45 cm depth in Klg04. Manganese typically shows a peak just below turbidites.

Figure 5: Ca/Ti correlation between cores Klg03, Klg04 and Klg06, located 100 km west of the Çınarcık Basin. The three curves car be precisely linked. An erosional event is highlighted in Klg04 at 80 cm depth. The offset at the top of core Klg03 is related to the mixed layer and to the turbidite tA.

Figure 6: Correlation of Klg03 and Klg04 according to Ca/Ti and Natural Remanent Magnetization (NRM) measurements. Interpreted turbidites correlation shows that there are more turbidites recorded in Klg03 than in Klg04 during the same time frame. Dashed lines represent the main Ca/Ti correlations according to Figure

5. The light gray line represents the erosional event recorded in Klg04. The thick dashed line represents the sapropelic layer occurrence. NRM values decrease under values of 1.10^{-2} A/m at 80 cm for Klg04 and at 200 cm for Klg03. The data are not considered relaible below these depths. Synchronous turbidites between the two cores are labelled with a capital E. XRF measurements were not acquired below 300 cm in Klg03 and Klg04 for technical reasons.

Figure 7: Excess ^{210}Pb activities (black dots), ^{137}Cs activities (diamond) and computed sedimentation rates of the cores Klg03 and Klg04. White dots along Klg04 are from a nearby Remote Operation Vehicle (ROV) core and show that no significant loss of sediments occurs in the cores during coring. The extent of the mixed layer is depicted with a line in Klg03. X-ray imagery associated to the mean grain size show the location of the turbidite likely induced by the 1894 earthquake. The turbidite is characterized by an increase in mean grainsize with an erosive base for both cores. In Klg03, two other disturbances are also visible in the X-ray and are related with an increase in mean grainsize. Turbidite tA, at 12 cm depth, is characterized by non-erosive laminae. Another small disturbance is observed at 30 cm depth without erosion. The occurrence of the peak in ^{137}Cs concentration would indicate that this turbidite is related to the M=6.3 1963 earthquake.

Figure 8: Cals3k.4 and Balkan reference curves for paleoinclination and paleodeclination are compared with the paleoinclination and paleodeclination records of Klg04 and Klg03. All sand bases of the turbidites have been removed. Mean of paleoinclination and paleodeclination data were obtained for the silt layer while all data were kept for hemipelagic sediments. The models show characteristic trends with periods

of low and high inclination. The same trends are observed for cores Klg04 and Klg03. Black lines represent standard deviation calculated for silt and hemipelagic layers.

Figure 9: Chronological model built by using OxCal software (Bronk Ramsey, 2007) for a ΔR of 400$\pm$50 years with Event E1 (1894 earthquake) puts as the initial boundary for the calibration. Data are arranged in stratigraphic order and turbidite-age modeled distributions are highlighted. Corresponding sample numbers are adjacent to each distribution (PDFs) where black lines correspond to the $2, \sigma$ standard deviation. Rectangles around some ages represented samples put in a phase function inside the OxCal mode.

Figure 10: Sediment-accumulation-rate curves for Klg03 and Klg04. Horizontal bars indicate the depth and age ranges of ^{14}C samples from the two cores. The Ca/Ti correlation (Fig. 5) allows for the transfer of ^{14}C ages from one core to the other. Vertical lines represent the interpolation of these turbidites based on the accumulation-rate curve. The age range is from the OxCal model. Arrows represent the depth of the synchronous turbidites between the two cores. Sedimentation rate for the different periods are indicated for both cores to the right of the curves.

Figure 11: Proposed rupture scenario for M>6.8 earthquakes in the Marmara Sea between 740 and 1999. Four sequences are observed but only three are complete. The 20^{th} Century westward propagation did not rupture the eastern Marmara Sea yet. The scenario is compatible with Coulomb stress analysis (Pondard et al., 2007) and description of damage (Ambraseys, 2002). Different shapes represent on-land and submarine paleoseismological investigations of NAF ruptures in and around the

Marmara Sea.

Figure A.1: Zijderveld diagram of demagnetization for cores Klg04 at 18 cm in depth and Klg03 at 160 cm in depth. The solid circles represent the projection on the horizontal plane and the open circles the projection on the vertical plane.

Figure A.2: Correlation between cores Klg03, Klg04 and C15 (Sarı and Çağatay, 2006). Ages are represented as uncalibrated.

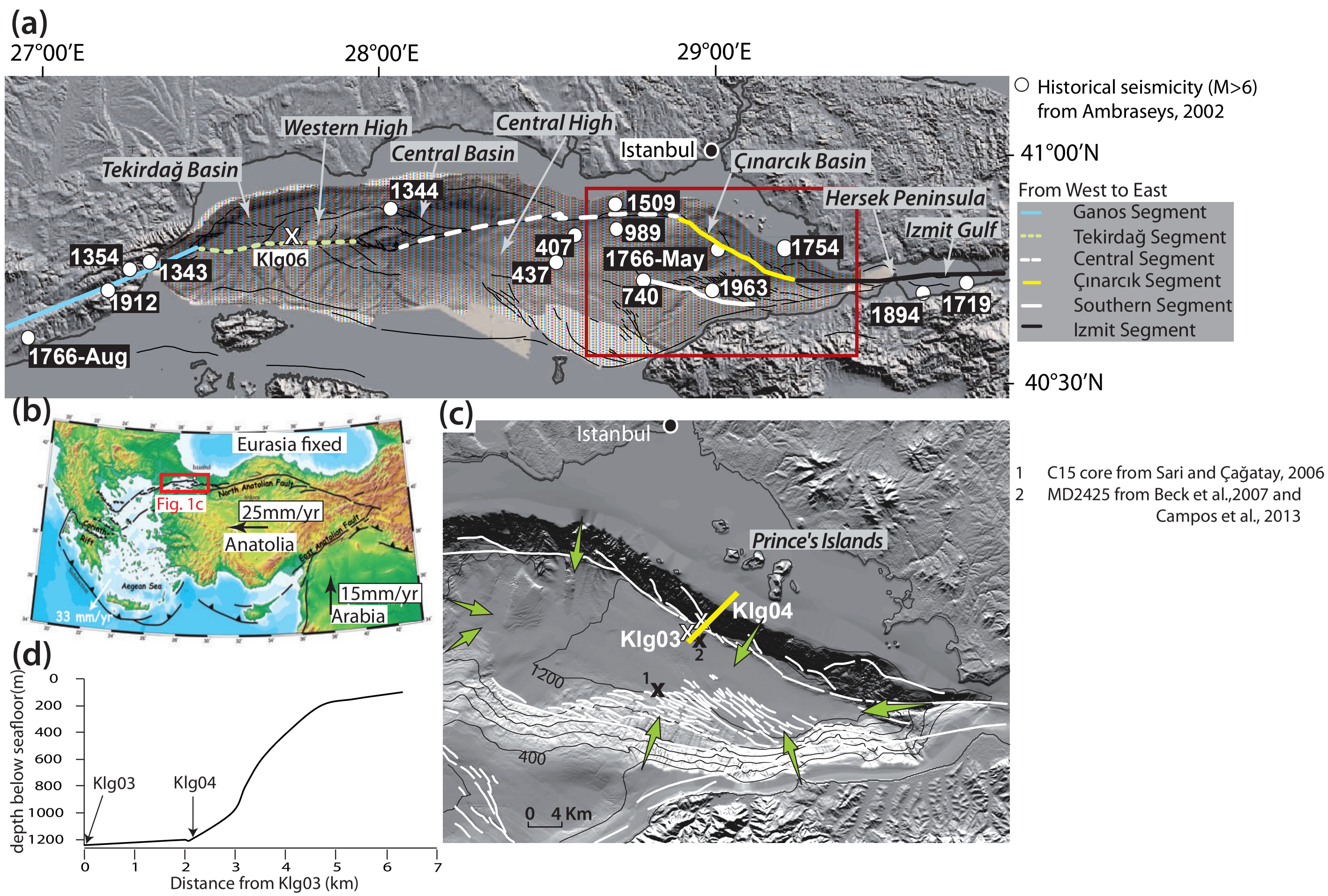

Figure 1: a/ General tectonic map of the Marmara Sea, crossed by the North Anatolian Fault (NAF). Basins, highs and main segments of the fault are indicated from the west to the east with different lines and their names are given in the gray box to the right. The study area is depicted with a box. Historical earthquakes located by Ambraseys (2002) are represented with a white dot. b/ Global geodynamic context of the Anatolian Plate with GPS velocities from Reilinger et al. (2006). The location of the Marmara Sea is indicated with a box. c/ Map of Çınarcık Basin and location of the two studied cores (Klg03 (40°47.98N; 28°59.55E) and Klg04 (40°48.60N; 29°00.73E) represented with a white cross) with respect to the Çınarcık Fault segment. Arrows show sediment paths for turbidite deposits (Altınok et al., 2011). The line crossing the two cores represent the path topographic profile presented in d/. Black crosses represent the location of other published cores discussed in the study. d/ Topographic profile of the northern part of the Çınarcık Basin. The profile starts at Klg03 core location.

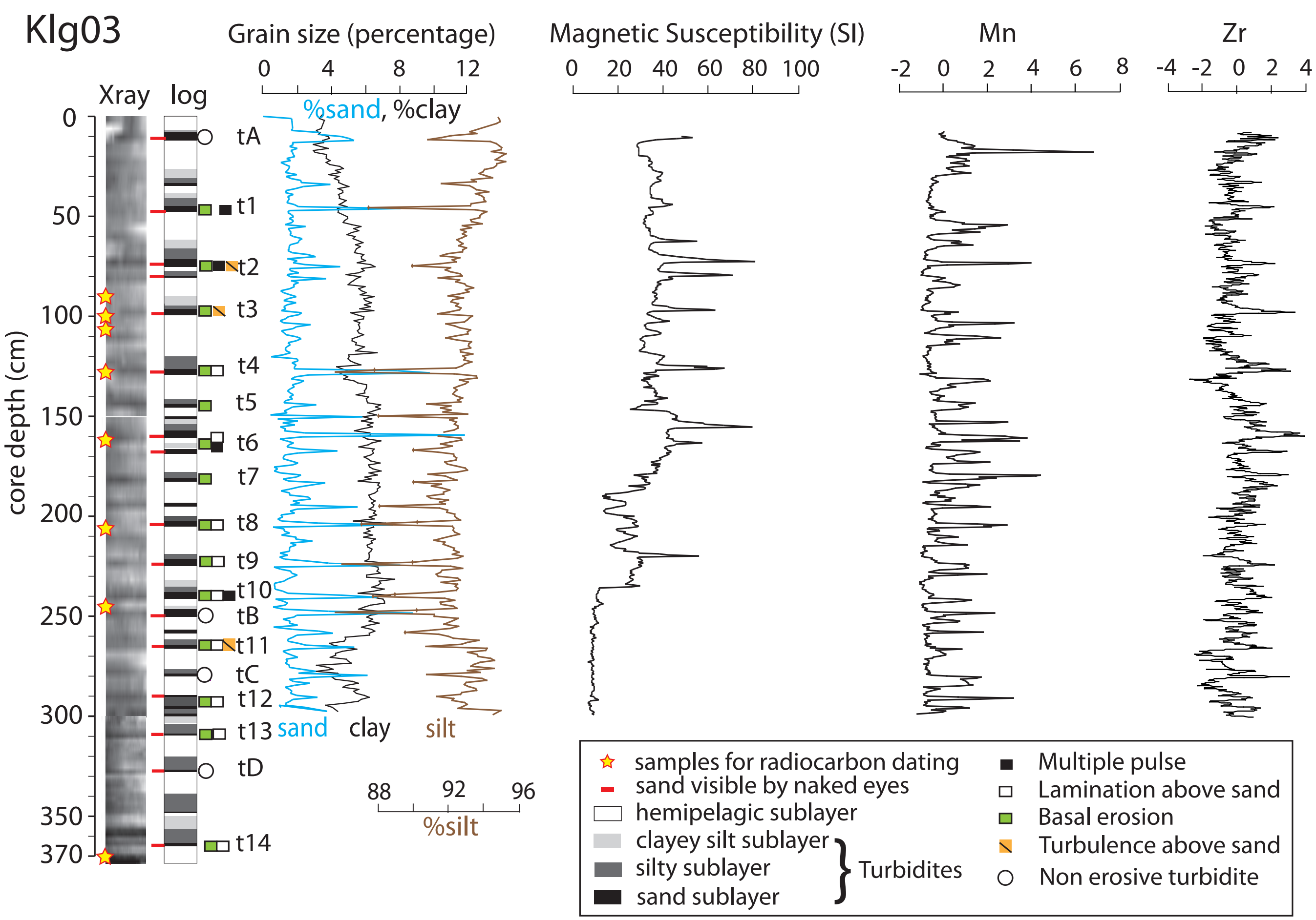

Figure 2: Stratigraphic obtained combining X-ray imagery, particle size, magnetic susceptibility data, Mn and Zr standardized intensities. Major erosive deposited turbidites are labelled, beginning with 1 at the top of the core. Sandy beds are depicted in black, intermediate silty beds in gray, upper clay-rich beds in light gray and hemipelagic sedimentation in white. Sand layers name is given when the percentage of sand is greater than the background percentage. Description of the turbidites seen in the X-ray radiographs is also given with different symbols on the right side of the core log. Turbidites without an erosive base are labelled with a letter.

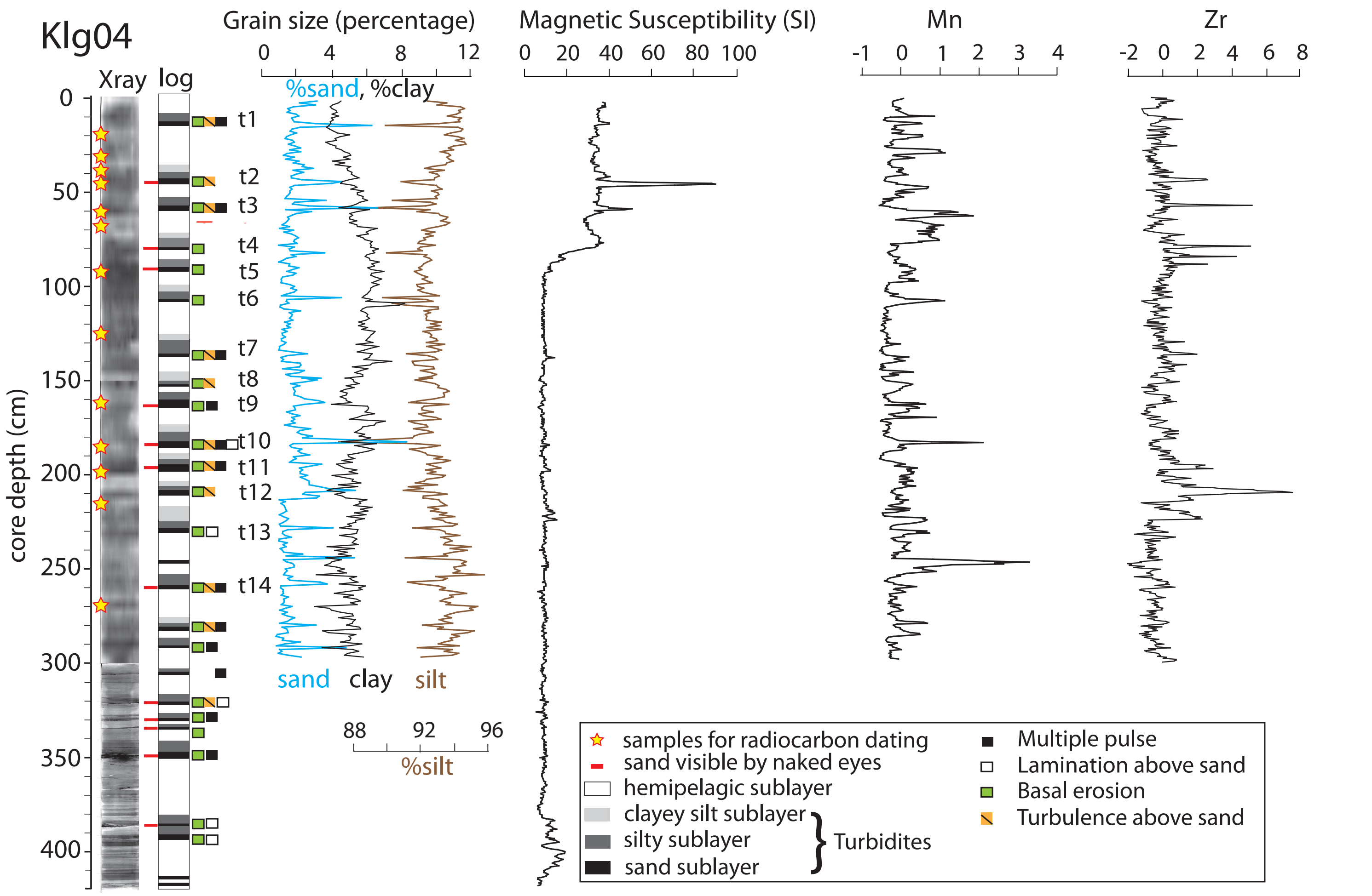

Figure 3: Stratigraphic obtained combining X-ray imagery, particle size, magnetic susceptibility data, Mn and Zr standardized intensities. Major erosive deposited turbidites are labelled, beginning with 1 at the top of the core. Sandy beds are depicted in black, intermediate silty beds in gray, upper clay-rich beds in light gray and hemipelagic sedimentation in white. Sand layers name is given when the percentage of sand is greater than the background percentage. Description of the turbidites seen in the X-ray radiographs is also given with different symbols on the right side of the core log.

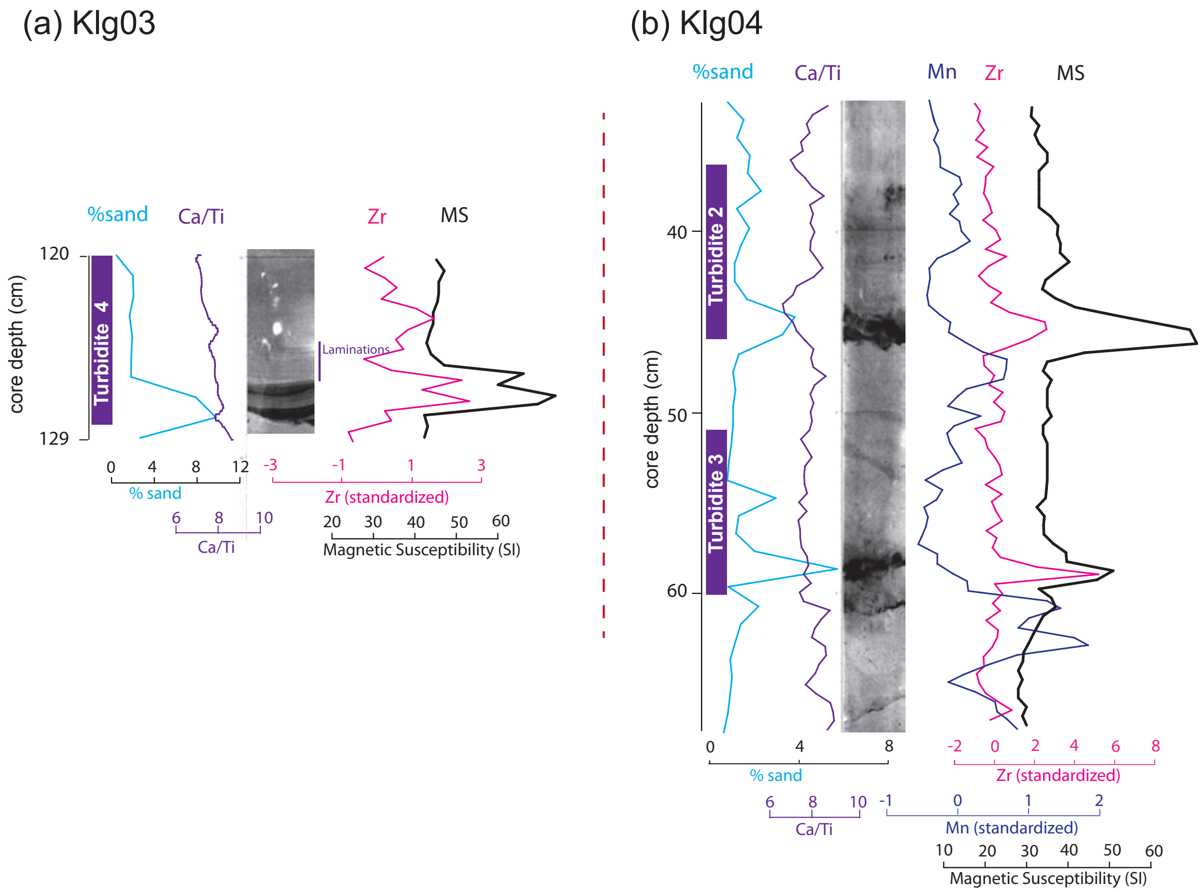

Figure 4: Typical examples of turbidites: granulometric and geochemical (Ca/Ti, Mn, Zr and MS) signatures. Turbidites are composed of a basal sand layer, an upper silt layer with frequent laminations and an upper light gray clayey layer. a/ X-ray imagery, granulometry and geochemical profiles of turbidite e4 at 120 cm depth in Klg03. b/ X-ray imagery, granulometry and geochemical profiles of turbidite e2 at 45 cm depth in Klg04. Manganese typically shows a peak just below turbidites.

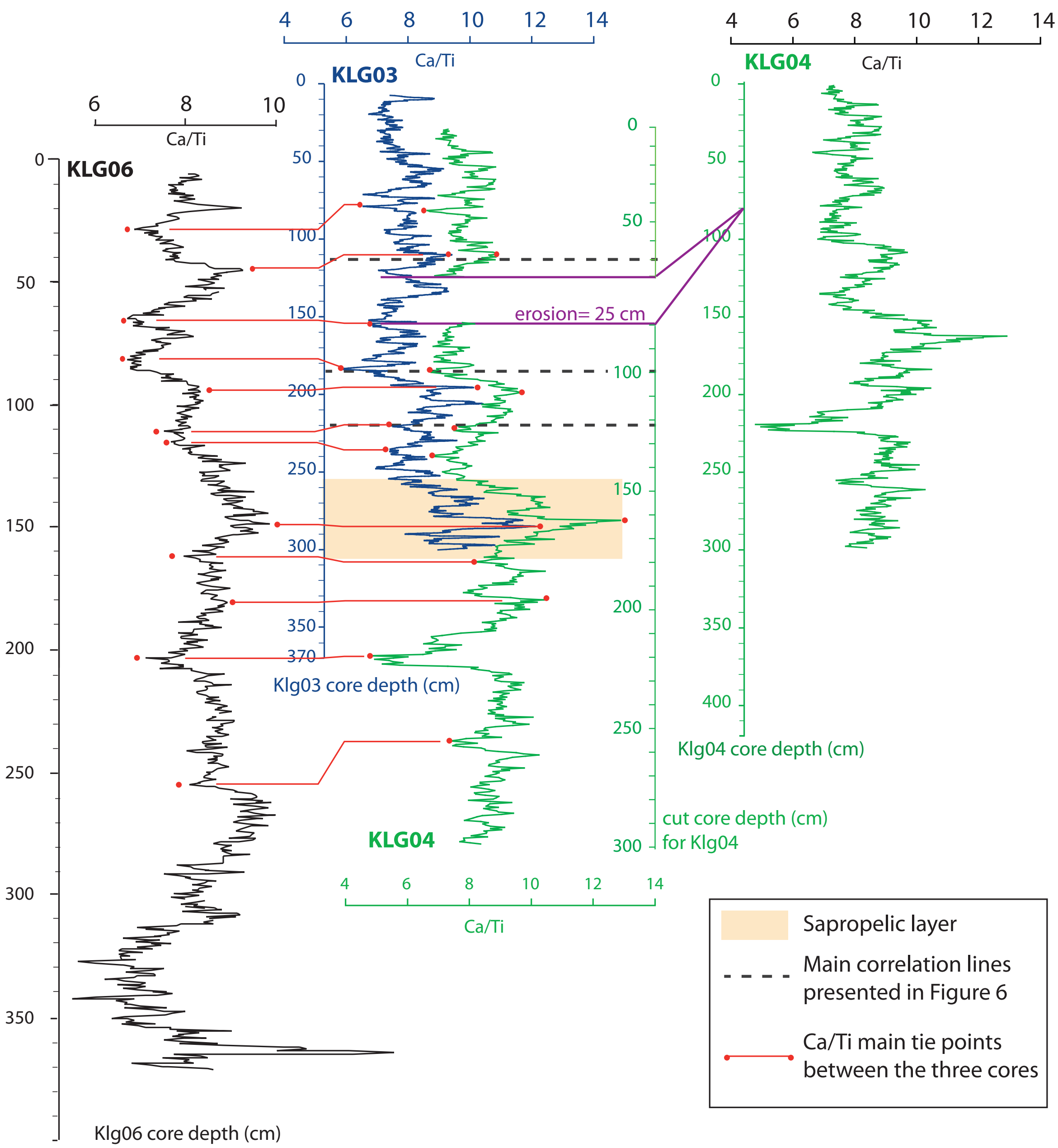

Figure 5: Ca/Ti correlation between cores Klg03, Klg04 and Klg06, located 100 km west of the Çınarcık Basin. The three curves car be precisely linked. An erosional event is highlighted in Klg04 at 80 cm depth. The offset at the top of core Klg03 is related to the mixed layer and to the turbidite tA.

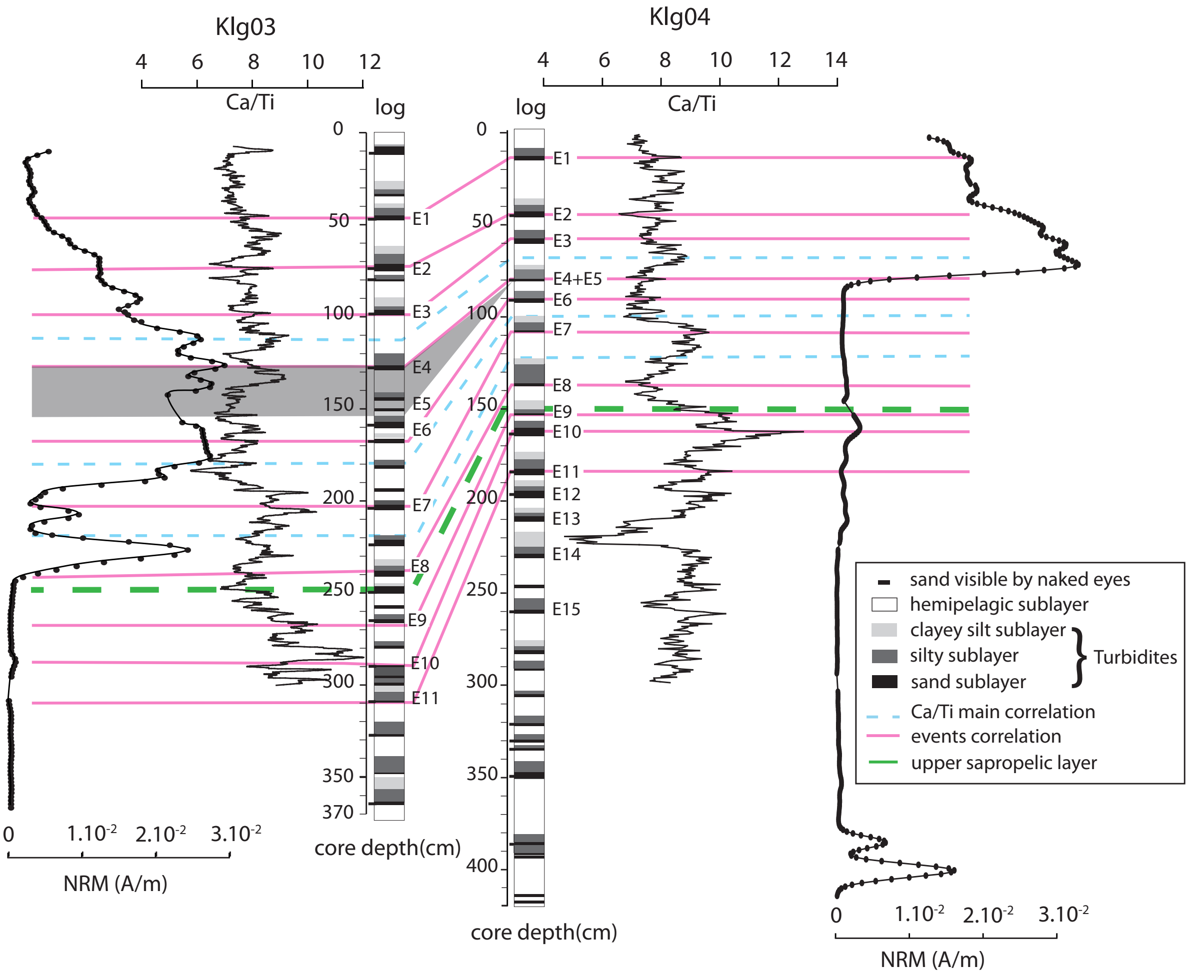

Figure 6: Correlation of Klg03 and Klg04 according to Ca/Ti and Natural Remanent Magnetization (NRM) measurements. Interpreted turbidites correlation shows that there are more turbidites recorded in Klg03 than in Klg04 during the same time frame. Dashed lines represent the main Ca/Ti correlations according to Figure 5. The light gray line represents the erosional event recorded in Klg04. The thick dashed line represents the sapropelic layer occurrence. NRM values decrease under values of 1.10^{-2} A/m at 80 cm for Klg04 and at 200 cm for Klg03. The data are not considered relaible below these depths. Synchronous turbidites between the two cores are labelled with a capital E. XRF measurements were not acquired below 300 cm in Klg03 and Klg04 for technical reasons.

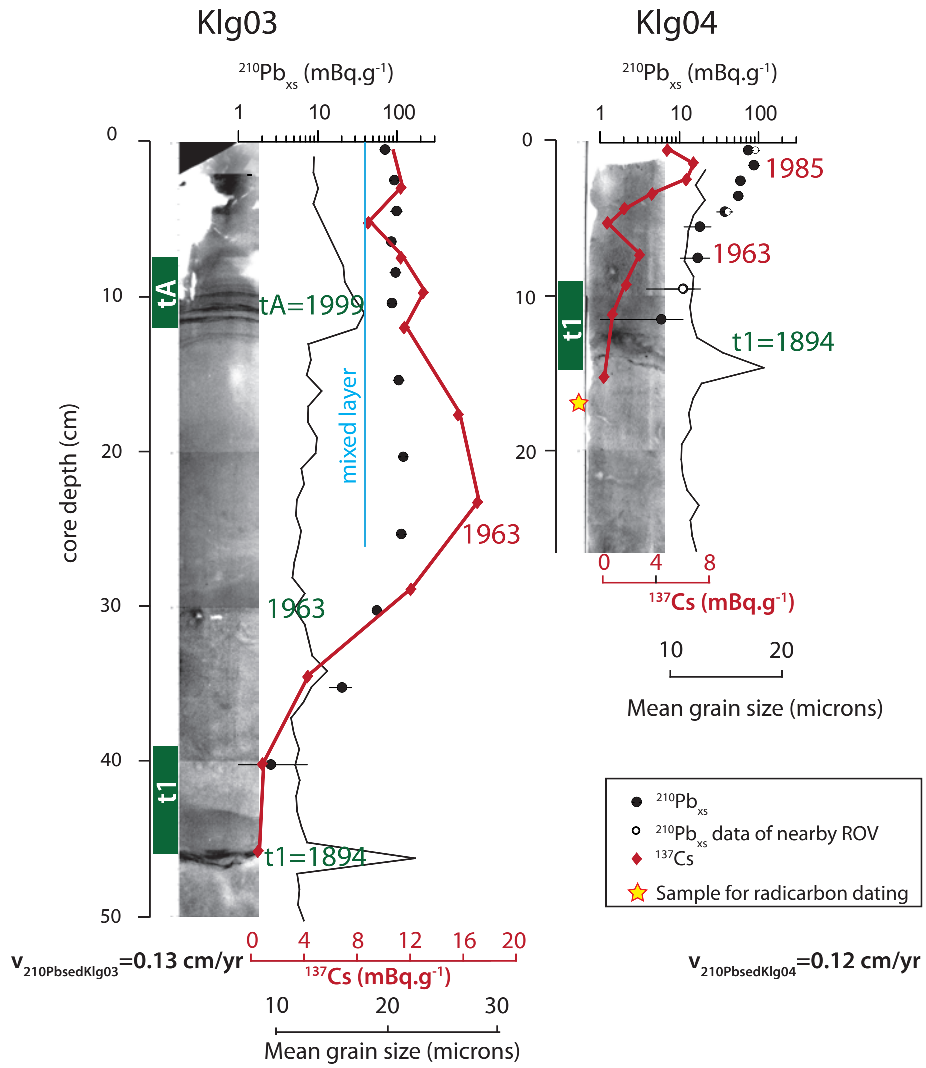

Figure 7: Excess ^{210}Pb activities (black dots), ^{137}Cs activities (diamond) and computed sedimentation rates of the cores Klg03 and Klg04. White dots along Klg04 are from a nearby Remote Operation Vehicle (ROV) core and show that no significant loss of sediments occurs in the cores during coring. The extent of the mixed layer is depicted with a line in Klg03. X-ray imagery associated to the mean grain size show the location of the turbidite likely induced by the 1894 earthquake. The turbidite is characterized by an increase in mean grainsize with an erosive base for both cores.

In Klg03, two other disturbances are also visible in the X-ray and are related with an increase in mean grainsize. Turbidite tA, at 12 cm depth, is characterized by non-erosive laminae. Another small disturbance is observed at 30 cm depth without erosion. The occurrence of the peak in ^{137}Cs concentration would indicate that this turbidite is related to the M=6.3 1963 earthquake.

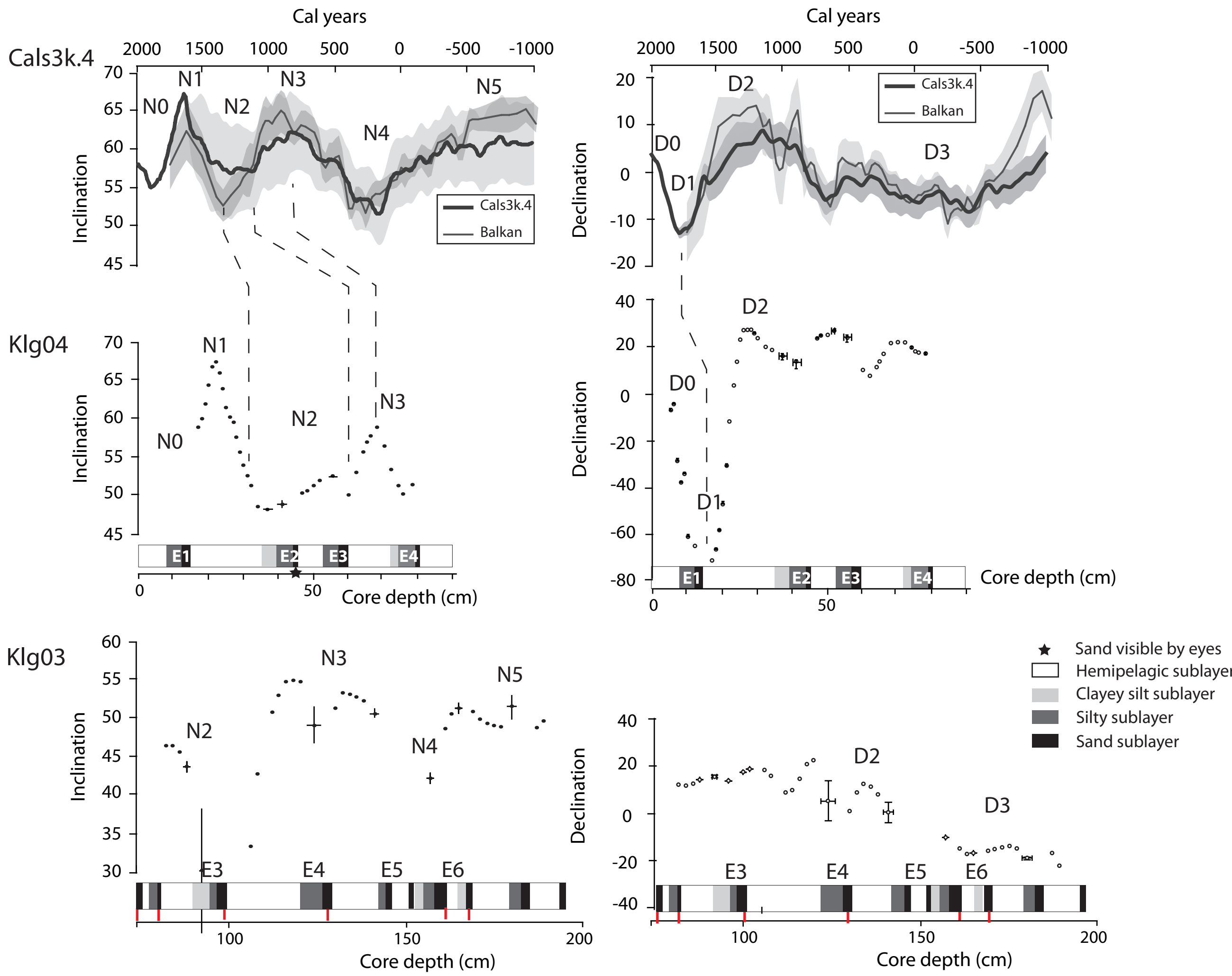

Figure 8: Cals3k.4 and Balkan reference curves for paleoinclination and paleodeclination are compared with the paleoinclination and paleodeclination records of Klg04 and Klg03. All sand bases of the turbidites have been removed. Mean of paleoinclination and paleodeclination data were obtained for the silt layer while all data were kept for hemipelagic sediments. The models show characteristic trends with periods of low and high inclination. The same trends are observed for cores Klg04 and Klg03. Black lines represent standard deviation calculated for silt and hemipelagic layers.

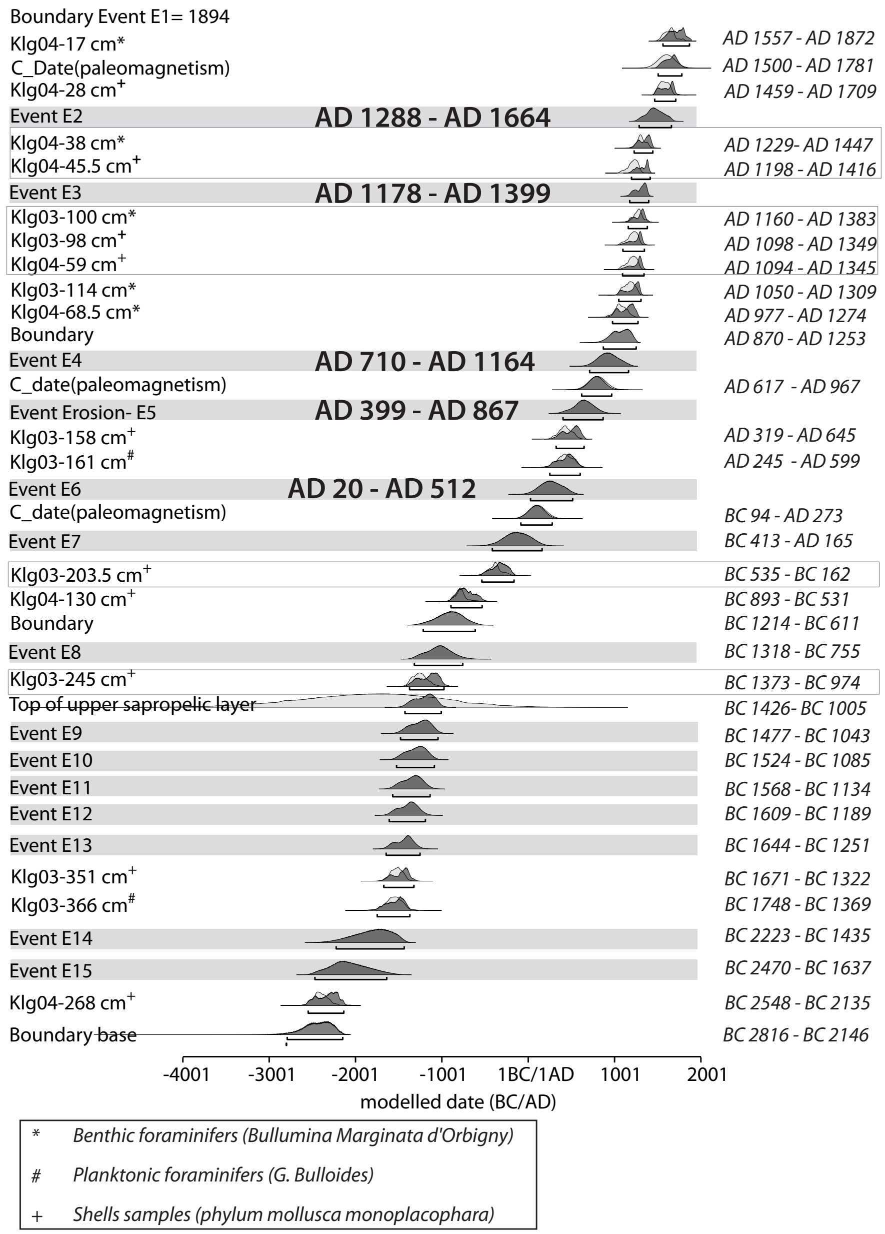

Figure 9: Chronological model built by using OxCal software (Bronk Ramsey, 2007) for a ΔR of 400$\pm$50 years with Event E1 (1894 earthquake) puts as the initial boundary for the calibration. Data are arranged in stratigraphic order and turbidites age modeled distributions are highlighted. Corresponding sample numbers are adjacent to each distribution (PDFs) where black lines correspond to the 2σ standard deviation. Rectangles around some ages represented samples considered as phase in the OxCal model.

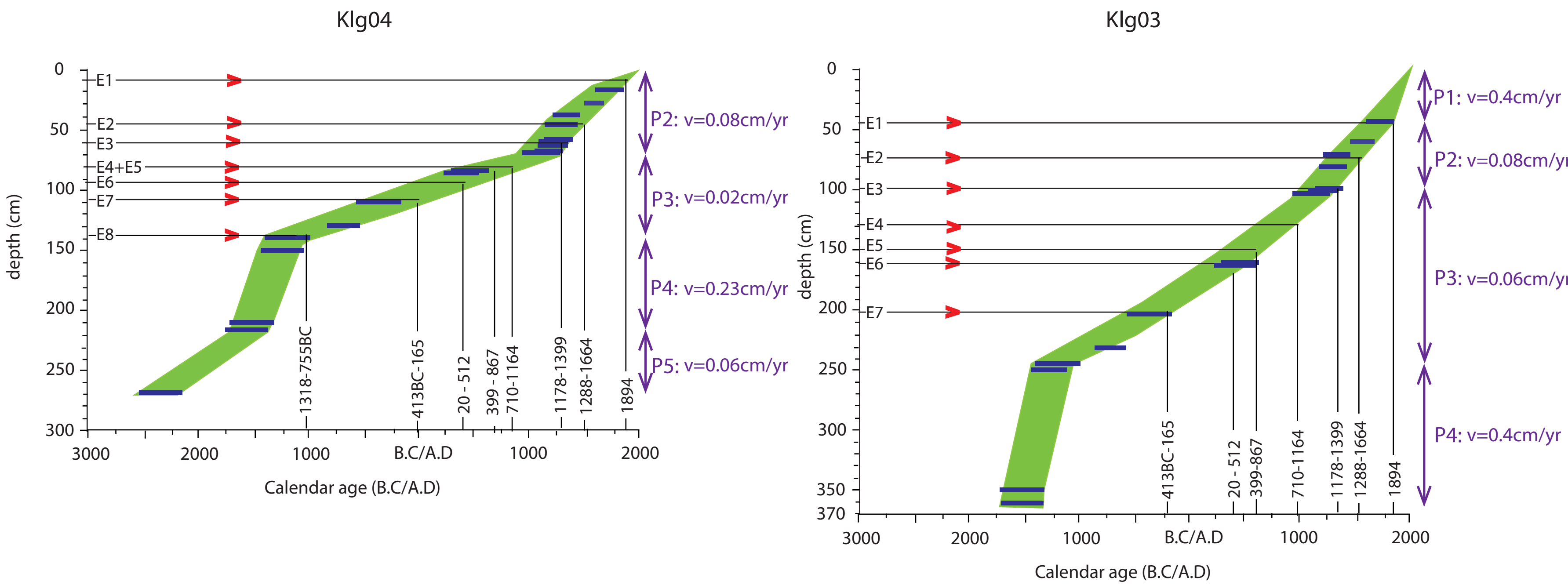

Figure 10: Sediment-accumulation-rate curves for Klg03 and Klg04. Horizontal bars indicate the depth and age ranges of ^{14}C samples from the two cores. The Ca/Ti correlation (Fig. 5) allows for the transfer of ^{14}C ages from one core to the other. Vertical lines represent the interpolation of these turbidites based on the accumulation-rate curve. The age range is from the OxCal model. Arrows represent the depth of the synchronous turbidites between the two cores. Sedimentation rate for the different periods are indicated for both cores to the right of the curves.

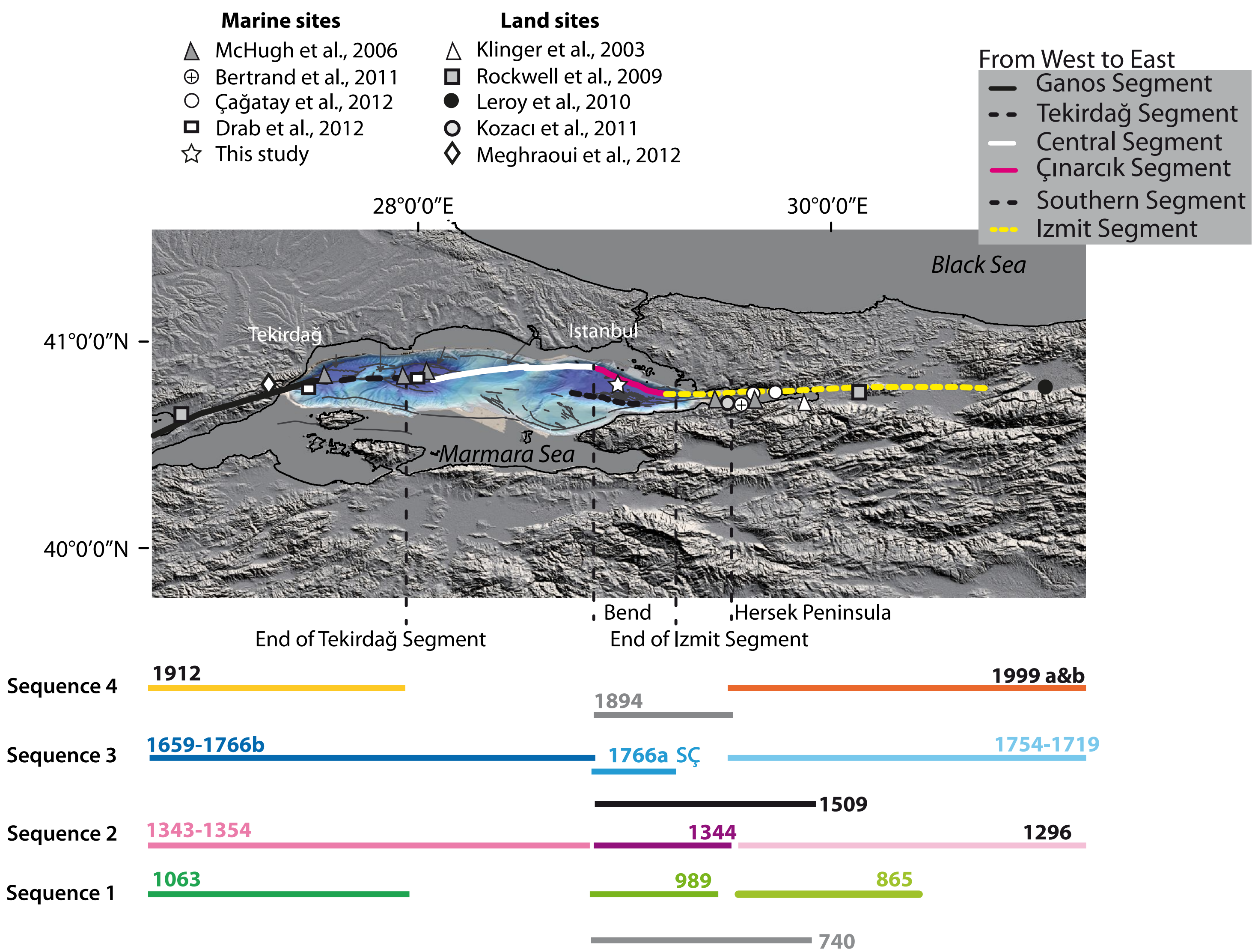

Figure 11: Proposed rupture scenario for M>6.8 earthquakes in the Marmara Sea between 740 and 1999. Four sequences are observed but only three are complete. The 20th Century westward propagation did not rupture the eastern Marmara Sea yet. The scenario is compatible with Coulomb stress analysis (Pondard et al., 2007) and description of damage (Ambraseys, 2002). Different shapes represent on-land and submarine paleoseismological investigations of NAF ruptures in and around the Marmara Sea.

Appendix

This appendix presents the Zijderveld diagrams for cores Klg03 and Klg04. The second figure presented displays the correlation between Klg03, Klg04 cores and C15 core previously studied by Sarı and Çağatay (2006).

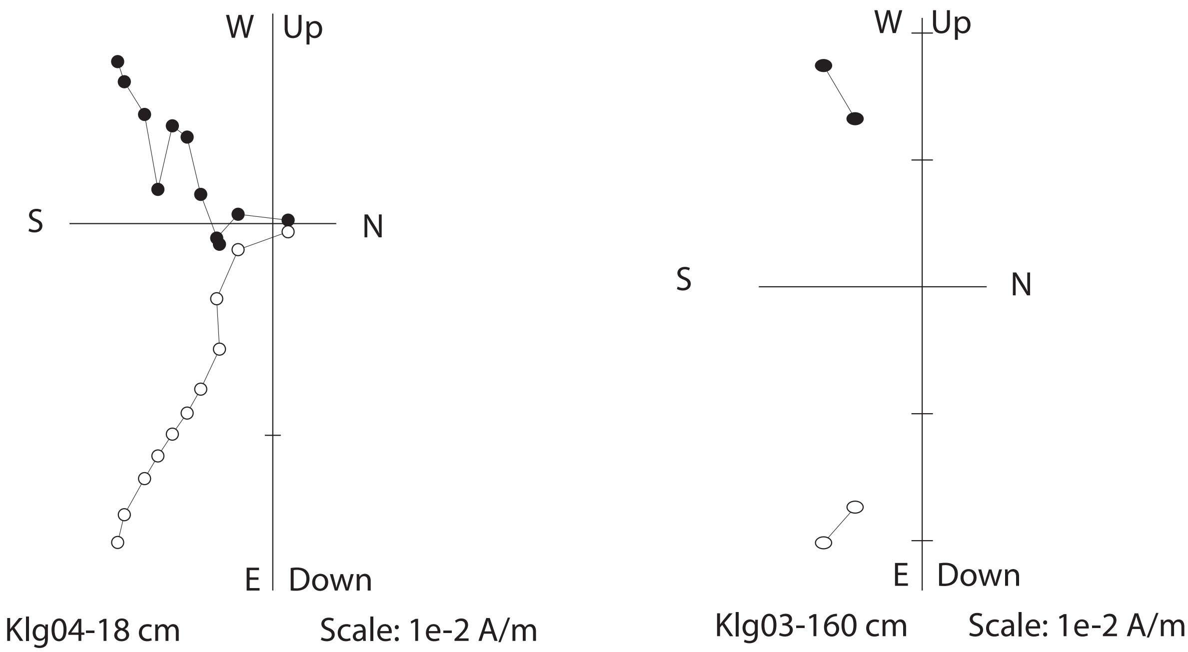

Figure A.1: Zijderveld diagram of demagnetization for cores Klg04 at 18 cm in depth and Klg03 at 160 cm in depth. The solid circles represent the projection on the horizontal plane and the open circles the projection on the vertical plane.

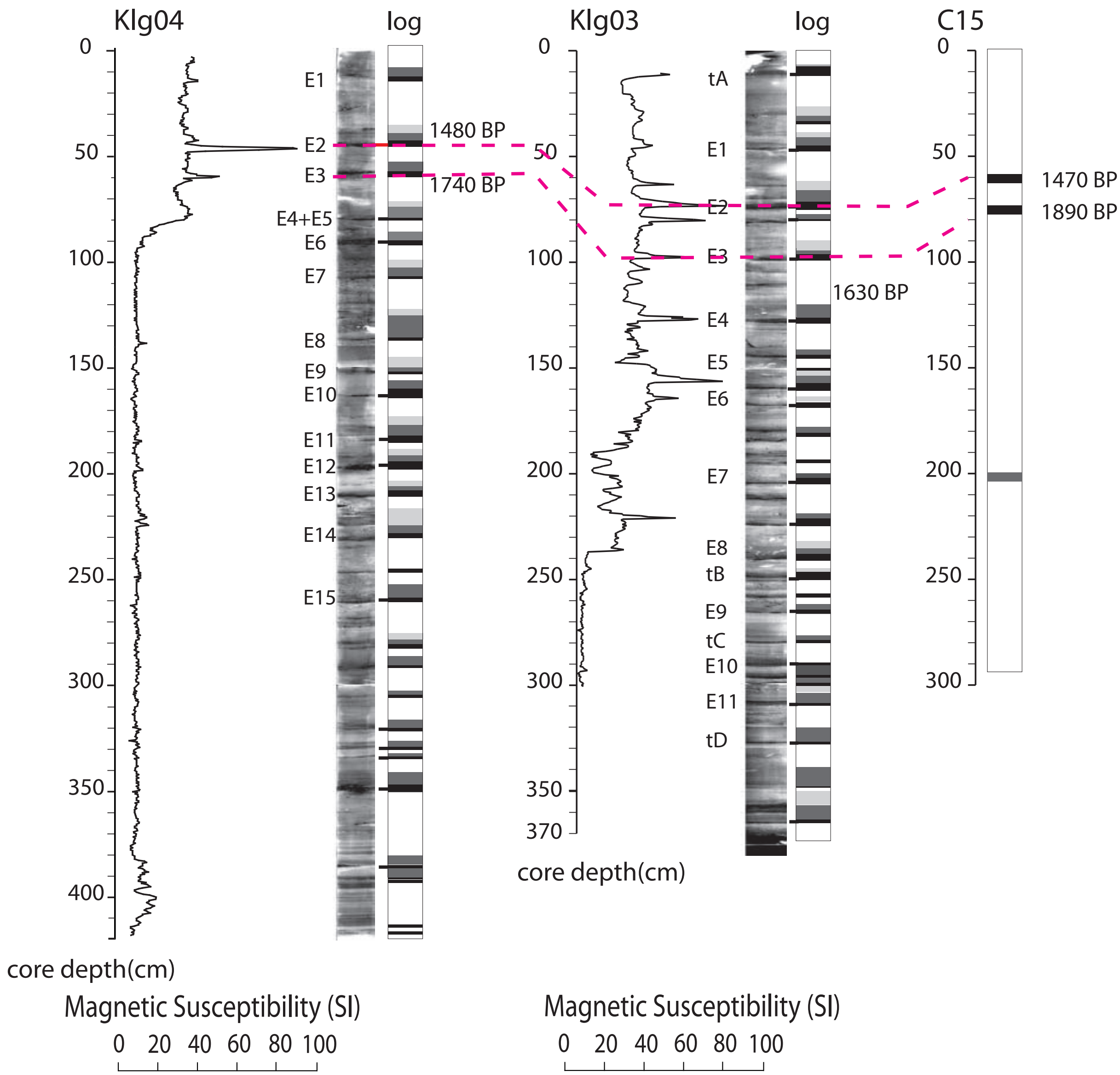

Figure A.2: Correlation between cores Klg03, Klg04 and C15 (Sarı and Çağatay, 2006). Ages are represented as uncalibrated.